CHAPTER 11

SPATIAL AND TEMPORAL PATTERNS IN MEASURED DATA

One of the objectives of PREVENT was to determine the spatial and temporal patterns of aerosol concentration and chemical composition which occurred in western Washington State during the summer of 1990. In this chapter, these patterns are examined systematically using empirical orthogonal function (EOF) analysis. EOF analysis reduces all observed spatial patterns for each measured parameter to a few typical patterns which explain most of the variance in the data. Also, the spatial and temporal patterns are examined using simple time plots of simultaneous measurements at the receptor sites, and by creating contour plots of mean concentrations for each species.

11.1 PARTICLE DATA

Details of the measurement methodologies for the fine particle data are discussed in Chapters 2 and 4. Table 2-1 gives the site locations and elevations of the particulate monitoring sites and Figure 11-1 is a map of these sites on the same scale which is used for all subsequent contour maps of particle data. Three sites, Marblemount in North Cascades National Park, and Paradise (high elevation) in Mount Rainier National Park and Tahoma Woods (low elevation) near Mount Rainier National Park, are receptor sites. Full IMPROVE samplers were deployed at these three sites. Module A only was deployed at the remaining 31 sites.

Twice daily 12-hour duration samples beginning at 8:00 am and 8:00 pm were collected at the three receptor sites. All other sites had 24-hour sample durations beginning at 8:00 am daily. For purposes of examining the spatial patterns among sites, data from the receptor sites were averaged to 24-hour durations.

The chemical species examined for spatial and temporal trends are fine mass and its major constituents including, sulfur, b_{abs}, and organic matter by hydrogen (OMH), and all trace elements for which there were sufficient data above the minimum detection limit (MDL).

Light absorption, b_{abs}, measured from the Teflon filter by the laser integrating plate method (LIPM) is expressed in units of concentration, assuming the absorption to mass ratio of light absorbing particles on the Teflon filter is 10 m^2/g. Absorption is usually assumed to be primarily due to light absorbing carbon, but other particles, including soil may also absorb light.

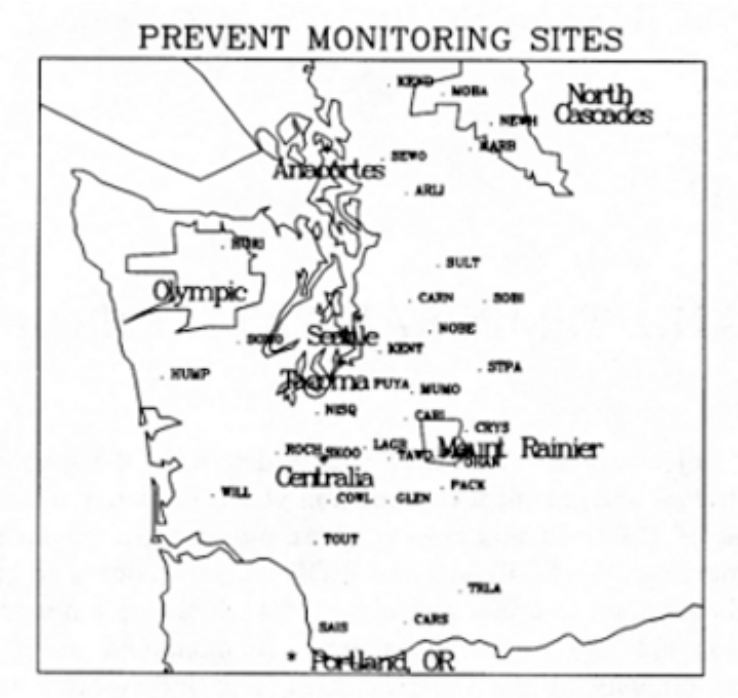

Figure 11-1. PREVENT particulate monitoring sites, national parks in Washington State, and major source areas. Scale is the same as all contour maps in this chapter.

OMH is calculated by:

$$OMH = 13.75\,(H - 0.25\,S). \tag{11-1}$$

The assumptions associated with this equation are discussed in Chapter 4.

Trace elements for which there were sufficient data above the MDL include: Al, Br, Ca, Cu, Fe, K, Mn, Na, Pb, V, Zn, Si, and Ti. Trace elements for which more then 70% of the observations were below the MDL are As, Co, Cr, Mg, Ni, Rb, Se, Sr, and Zr. No EOF analyses of these data were attempted. X-ray Fluorescence (XRF) analysis of the Teflon filters from the receptor sites provided higher sensitivity for several trace elements at these three sites. However, PIXE data only was available for all other sites. Therefore, for consistency between sites, only data obtained from PIXE was used for the EOF analysis.

11.2 METHODOLOGY

11.2.1 Relationship of EOFs to Spatial Patterns

Empirical orthogonal function (EOF) analysis can be used to systematically examine the spatial and temporal patterns in measured concentrations (or other data) across several monitoring sites in a region. While these patterns can be observed simply by creating isopleth maps of the

concentrations for each measurement period, EOF analysis has the advantage of simplifying these many maps into a few patterns (EOFs) which can be linearly recombined to reproduce the observations for all time periods.

A single data matrix (time by site) of pollutant concentrations is decomposed into two matrices, one independent of time (EOF by site) and the other independent of location (time by EOF). Multiplication of the resulting two matrices regenerates the original matrix.

The EOF by site matrix can be thought of as a series of isopleth maps (one for each EOF), of common concentration patterns in space, while the time by EOF matrix, plotted as a series of time plots, also one for each EOF, reveals the relative importance of each EOF for each sampling period. The advantage of the analysis is that while there are as many EOFs as there are sites, in general only a few are needed to explain most of the variance in the data.

The EOF analysis is useful because there are usually only a few similar physical conditions that occur during a field study in a given region and time period. For example, one hypothetical condition might be stagnation around the pollutant sources with low wind speeds and relatively little transport. In this case the concentrations near sources would be much higher than the concentrations at receptors farther distant from any source. Another condition which occurs during the same study might be moderate westerly winds that transport pollutants eastward. In this case, receptors west of sources would have low or zero concentrations. Receptors east of sources would have concentrations which decreased as the distance from the source increased. These are simple examples. In the real world, interpretation of spatial concentration patterns is complicated by other factors such as complex terrain, changing emission rates, and variables affecting chemical transformation such as relative humidity, clouds, and temperature.

Although identical meteorological and chemical conditions will never occur repeatedly, in general, all spatial patterns in the pollutant concentrations can be expressed as linear combinations (with different weights for each spatial pattern for each monitoring period) of just a few conditions which occur repeatedly in a similar manner. Sources are usually located near areas where the spatial gradients in the concentration field (and EOF field) are largest.[1] The EOF analysis does not explicitly reveal the physical conditions which are associated with each spatial pattern in the concentrations, but often the physics can be inferred as described in the examples above. The hypotheses can then be further investigated by examining additional information, such as meteorology, inter-species relationships, etc.

11.3 PROCEDURE

A matrix of centered concentrations of a single chemical species (mean for the site subtracted from each concentration) is decomposed into two matrices as follows:

$$Z = A \times P \tag{11-2}$$

where:

Z = Centered concentration matrix with the rows corresponding to times of observation and columns to locations.

A = Orthonormal matrix of dimensionless time weighing factors. Rows correspond to time periods and columns correspond to EOFs.

P = Orthogonal matrix of spatial EOFs. Rows are EOFs, columns correspond to sites. Values are weighted deviations from the mean concentration at each site.

P is the matrix of eigenvectors of Z^TZ multiplied by the matrix which contains the square roots of the eigenvalues of Z^TZ on the diagonal and zeros elsewhere. The eigenvalues have units of concentration squared so entries in the P matrix are units of concentration. A is found by postmultiplying the centered data, Z, by the inverse of P. More details of the decomposition can be found in texts on multivariate analysis.[2,3]

EOFs are orthogonal, statistically simple, and each explains a decreasing amount of the total variance, but they are not a unique decomposition of the data and frequently the patterns associated with each are more physically interpretable and better represent the patterns in the input data after rotation. The advantages and disadvantages of orthogonally and obliquely rotated and unrotated EOFs are discussed in detail by Richman.[4] For this study, the EOFs were rotated using the Varimax criteria which forces each site to load as strongly as possible onto one EOF while loading weakly onto all others.[5] This can be useful for determining the source areas and meteorological conditions which most influence each site. The number of factors to rotate was determined by the number of eigenvalues of the correlation matrix which were greater than one.

11.4 MISSING DATA

Data must exist for every site for every time period which is included in an EOF analysis. Data collection at most PREVENT sites began June 21, 1990, and ended September 3, 1990. However, nine sites had missing data on September 3, and data collection at two sites, Sauvie Island and Paradise did not begin until July 18 and 20, respectively. Therefore, to include all sites, the time period chosen for analysis was July 20 through September 2, 1990.

Two steps were taken to deal with missing data during this analysis period. First, missing concentrations preceded and followed by valid data at the same site were filled by linear interpolation across time. Approximately 1% of the data were filled in this way. Other missing data were replaced by a distance weighted (inverse of the squared distances) average of concentrations at sites with non-missing data for the same time period. Approximately 2% of the data were replaced by this method.

Concentrations below the MDL were set to zero. Of the species chosen for EOF analyses, the highest percent of data below the MDL were vanadium (23.4%), aluminum (23.7%), and copper (14.7%). Less than 8% of the concentrations of all other species were below the MDL. Table 11-1 summarizes the number of missing and below MDL concentrations for each species and shows how many of the missing data were filled by each of the two methods discussed above.

Table 11-1. Number of missing observations filled by each method and number of observations below MDL for each species. Total number of observations for each species are (45 days)x(34 sites)=1530.

Species	Time Interpolation	Spatial Interpolation	Below Minimum Detection
Aluminum	16 (19%)	37 (2%)	362 (24%)
b_{abs}	17 (19%)	37 (2%)	0 (2%)
Bromine	16 (19%)	37 (2%)	23 (2%)
Calcium	16 (19%)	37 (2%)	8 (1%)
Copper	16 (19%)	37 (2%)	225 (15%)
Fine mass	21 (19%)	39 (3%)	0
Iron	16 (19%)	37 (2%)	0
OMH	16 (19%)	37 (2%)	0
Lead	16 (19%)	37 (2%)	101 (7%)
Manganese	16 (19%)	37 (2%)	113 (7%)
Potassium	16 (19%)	37 (2%)	0
Silicon	16 (19%)	37 (2%)	5 (0%)
Sodium	16 (19%)	37 (2%)	136 (9%)
Sulfur	16 (19%)	37 (2%)	0
Titanium	16 (19%)	37 (2%)	77 (5%)
Vanadium	16 (19%)	37 (2%)	358 (23%)
Zinc	16 (19%)	37 (2%)	3 (0%)

11.5 RESULTS

11.5.1 Fine Mass

A contour plot of the mean fine mass at each of the 34 sites is shown in Figure 11-2. Mean concentrations greater than 12 $\mu g/m^3$ occurred at three sites, Puyallup, Kent, and Sultan. The mean concentrations in general decreased outward from these three sites except for a locally high value at Tahoma Woods (11.6 $\mu g/m^3$). The mean concentrations at the other two receptor sites were 7.6 and 9.4 $\mu g/m^3$ at Paradise, and Marblemount, respectively.

Time lines of the fine mass concentrations at the three receptor sites are shown in Figure 11-3. The highest concentrations at Tahoma Woods occurred on July 29 (23.2 $\mu g/m^3$) and August 2 (23.1 $\mu g/m^3$). The highest concentration at Paradise was 16.7 $\mu g/m^3$ on August 12 and the highest values at Marblemount were 18.4 $\mu g/m^3$ on August 5 and 18.0 $\mu g/m^3$ on August 14.

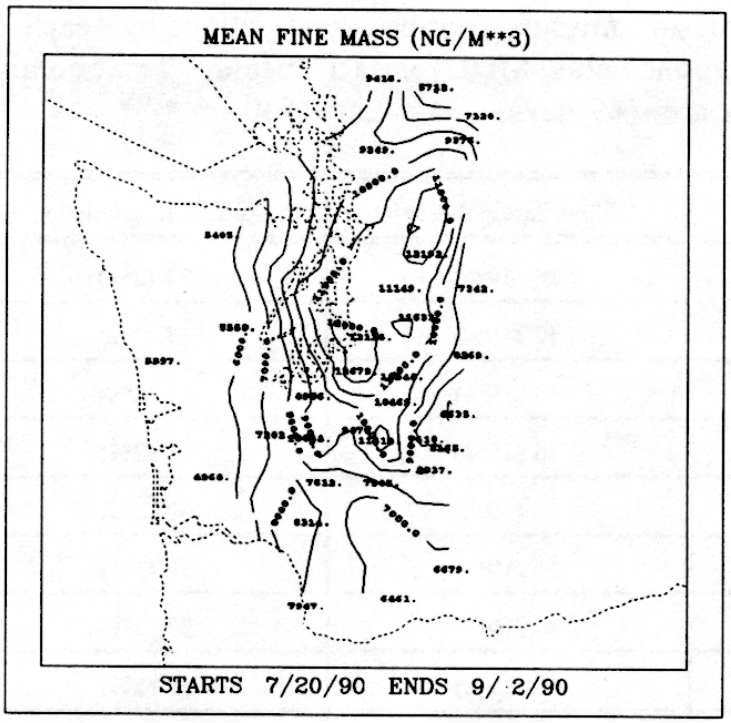

Figure 11-2. Contour plot of mean fine mass. Contour interval is 1000 ng/m^3.

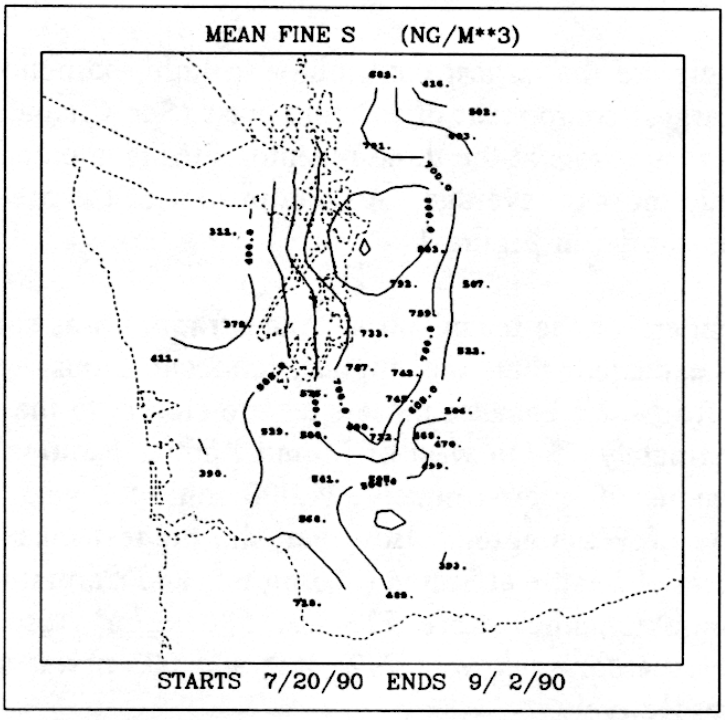

Figure 11-3. Time line of fine mass concentrations at the three receptor sites.

The EOFs of fine mass are not presented because more information can be gained by examining the spatial patterns associated with the major constituents of the fine mass.

11.5.2 Sulfur

Sulfate aerosols are the largest contributor to light extinction at the three receptor sites and are the second largest component of the fine mass (See Chapter 6). The fraction of sulfate associated with marine aerosols at the three receptor sites is apparently quite low, about 10% or less of the total sulfate mass on average. A contour plot of the mean fine sulfur concentrations across the network is shown in Figure 11-4.

The spatial pattern of the mean sulfur concentrations was somewhat surprising. Prior to the study, it was expected that the highest concentrations would be observed around Skookumchuck and Rochester because these sites are closest to the Centralia Power Plant. The plant, located approximately 75 km west of Mount Rainier National Park, has estimated annual sulfur dioxide emissions of approximately 74,000 tons per year, or nearly half of the SO_2 emissions in the state of Washington. However, the highest mean sulfur concentrations were observed east and north of Seattle at Sultan (803 ng/m^3) and Carnation (792 ng/m^3). Mean values at Rochester and Skookumchuck were 529 and 580 ng/m^3, respectively. The mean sulfur concentrations at the receptor sites were 732, 468, and 603 ng/m^3 at Tahoma Woods, Paradise, and Marblemount, respectively.

Time plots of the sulfur concentrations at the receptor sites are shown in Figure 11-5. The most dramatic high sulfur episode at Mount Rainier National Park was August 12-14 when the 24-hour average elemental sulfur concentrations remained at around 1.3 μg/m^3 at Paradise for three days. Sulfur concentrations at Tahoma Woods were also at the maximum for that site during this time period, ranging from 1.0 to 1.4 μg/m^3. A second episode with slightly lower concentrations occurred during August 23 and 24 when sulfur concentrations at Tahoma Woods were 1.2 and 1.0 μg/m^3, respectively, while the values at Paradise were only slightly lower at 1.1 and 0.9 μg/m^3. Sulfur concentrations greater than 1 μg/m^3 at Marblemount in North Cascades National Park occurred on several days, including July 23, 24, 27, and 31, and on August 1 and 20.

A total of six sulfur EOFs were retained for rotation. The maps of the first three, explaining a total of 63.3% of the variance are shown in Figures 11-6 through 11-8 and the corresponding time factors are shown in Figure 11-9. EOF 1, explaining 26.8% of the variance has the highest values in the center of the network around the Seattle-Tacoma urban area, with the strongest gradients surrounding the central core on the east, north and west. This pattern appears to be indicative of stagnation. Apparently, sulfur emitted in the urban areas is mostly remaining in the urban areas, with minimal transport outward. This could be due to either low wind speeds or could result from winds with frequently changing direction, such as the land-sea and/or mountain-valley winds which would be expected from the geography in the area. This EOF pattern indicates that emissions from Centralia Power Plant may often become a part of the Seattle-Tacoma urban air mass and that other sources of sulfur in the urban area may be individually or collectively as important as Centralia in influencing the sulfur concentrations in

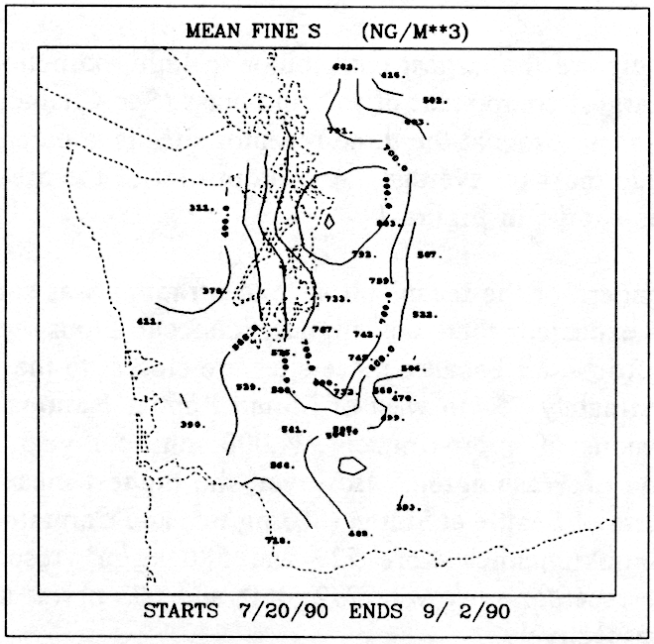

Figure 11-4. Contour plot of mean fine sulfur. Contour interval is 100 ng/m^3.

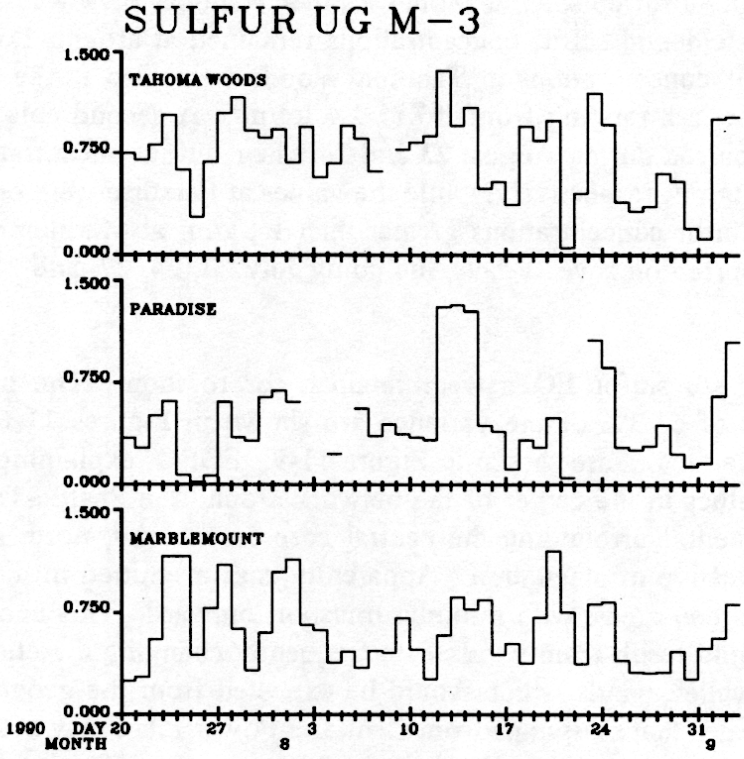

Figure 11-5. Time line of sulfur at the three receptor sites.

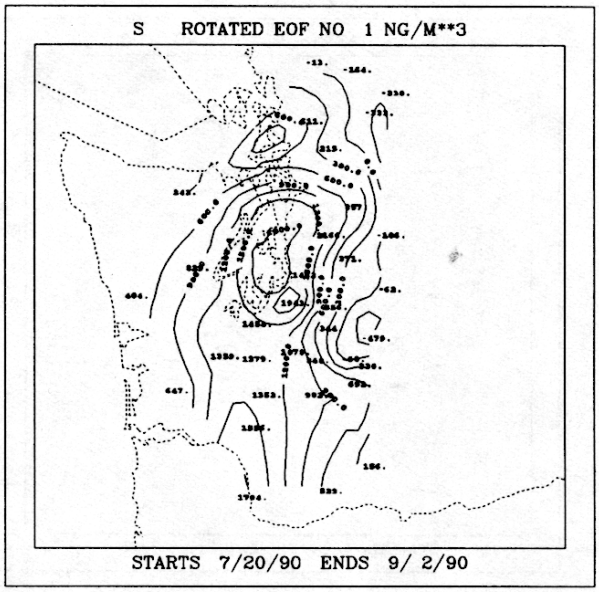

Figure 11-6. Rotated EOF 1 for sulfur explaining 26.8% of the variance. Contour interval is 300 ng/m^3.

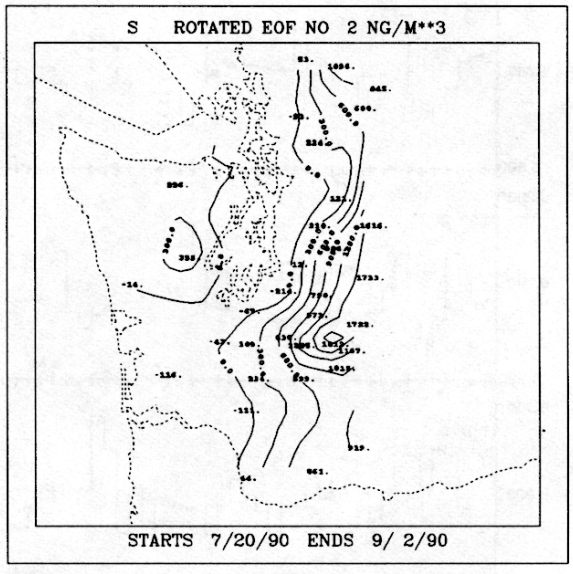

Figure 11-7. Rotated EOF 2 for sulfur explaining 22.4% of the variance. Contour interval is 300 ng/m^3.

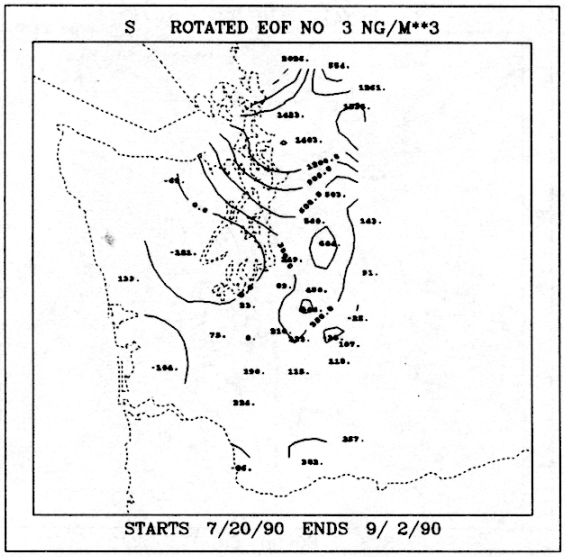

Figure 11-8. Rotated EOF 3 for sulfur explaining 14.1% of the variance. Contour interval is 300 ng/m^3.

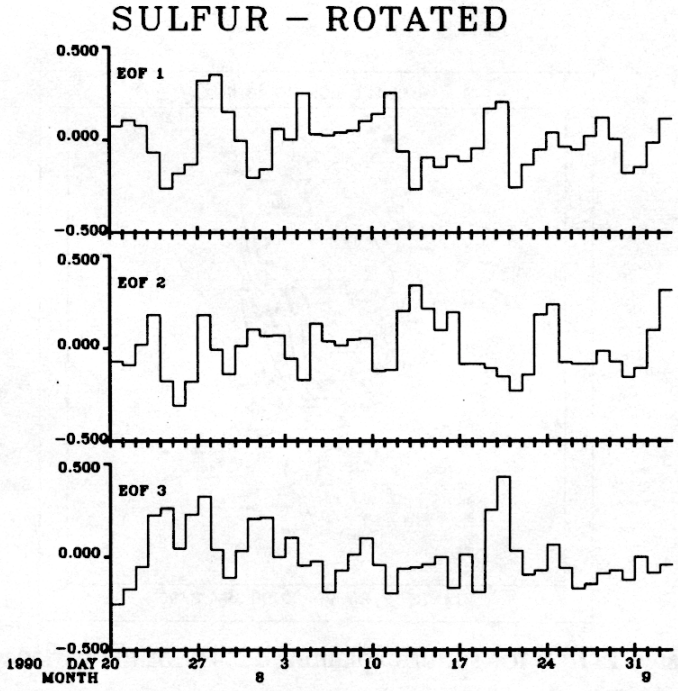

Figure 11-9. Time factors for first three rotated sulfur EOFs.

the region. Also of note in EOF 1 is the concentration gradient north of Seattle. This could be due to transport from Canada or be due to oil refining in Anacortes.

The second EOF, explaining 22.4% of the variance has the largest gradient along the western edge of the Cascade Mountain Range. Like EOF 1, this pattern also suggests that the sources which influence it are west of the Cascade Range. In this case the emissions appear to be transported toward the mountains by westerly winds. The air mass is then apparently blocked from further eastward movement by the high terrain. The correlation between the time factors for EOF 2 and the sulfur concentrations at Paradise is 0.87. The implication is that sulfur concentrations at Paradise, which has a relatively high elevation, will be higher when the westerly wind speeds are great enough to transport emissions from the Seattle-Tacoma-Centralia area westward as far as Paradise.

The third EOF, explaining 14.1% of the variance, has a north to south gradient which suggests a source area north of the study area, perhaps in Canada, or in the northern half of the network, possibly oil refining in Anacortes, WA. The correlation between the time factors for EOF 3 and the sulfur concentrations at Marblemount is 0.84, indicating that sulfur concentrations at this site are likely to be associated with transport from the north. Conversely, the correlations between the EOF 3 time factors and sulfur concentrations at Paradise and Tahoma Woods are only 0.01 and 0.16, respectively.

The correlations between sulfur concentrations at Tahoma Woods and the time factors for EOFs 1, and 2 are 0.43, and 0.61, respectively, indicating that sulfur concentrations there are more likely to be associated with transport from the west than from the north.

11.5.3 Organic Matter

The largest fraction of the fine mass is organic matter (See Chapter 6), and as expected, the contour plot of the mean values of OMH, as shown in Figure 11-10 closely resembles the contour plot of mean fine mass. The highest mean concentrations were at Puyallup (6.4 $\mu g/m^3$), North Bend (6.1 $\mu g/m^3$) and Sultan (5.8 $\mu g/m^3$), with values generally decreasing outward from these sites. The mean values at the receptor sites were 4.9 $\mu g/m^3$ at Tahoma Woods, 2.9 $\mu g/m^3$ at Paradise, and 4.4 $\mu g/m^3$ at Marblemount.

The time plot of OMH concentrations at the receptor sites is shown in Figure 11-11. Concentrations greater than 10 $\mu g/m^3$ occurred at Tahoma Woods on five days including July 21, July 28-29, August 11, and August 14. The highest OMH concentration at Paradise was 7.9 $\mu g/m^3$ which occurred on August 12. Episodes of OMH concentrations greater than 4 $\mu g/m^3$ at Paradise occurred on July 20-22, July 28-29, August 7-8, August 11-12, and August 28. At North Cascades NP, the highest concentration measured at the Marblemount site was 10.0 $\mu g/m^3$ on August 3. An additional three days had concentrations greater than 7 $\mu g/m^3$, including July 22 and 30, and August 4. The highest OMH concentrations at Tahoma Woods and Paradise were sometimes on the same day or the day preceding the highest sulfur concentrations at the same site, but this was not always true. Days of highest OMH and highest sulfur did not usually coincide at Marblemount.

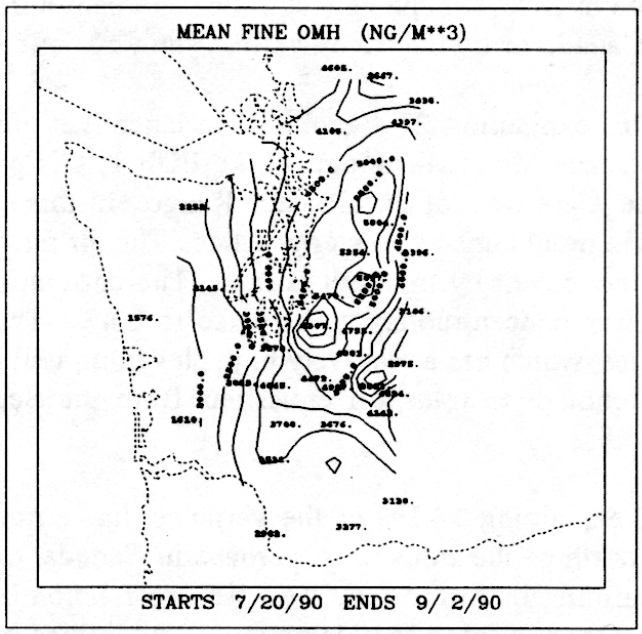

Figure 11-10. Contour plot of mean fine OMH. Contour interval is 500 ng/m^3.

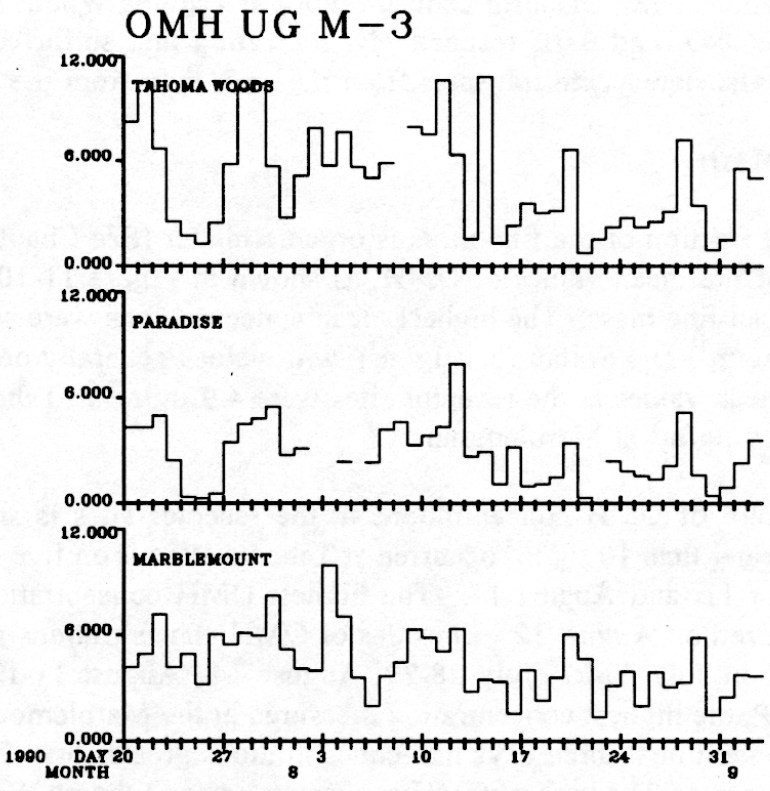

Figure 11-11. Time line of OMH at the three receptor sites.

Four EOFs, explaining a total of 82.3% of the variance were rotated for OMH. These are shown in Figures 11-12 through 11-15, and the corresponding time factors are shown in Figure 11-16. The first EOF seems to indicate an urban source for organic matter, although the highest values on the OMH EOF 1 map are farther south than for sulfur EOF 1, perhaps indicating the Tacoma area rather than Seattle is a source region for organics. Again, as for sulfur, the area of highest gradient circles the urban areas and is indicative of stagnation and either low wind speeds or diurnal land-sea and/or mountain-valley winds. Also of note for EOF 1 is the cyclic nature of the time factors. The cycle appears to be approximately weekly, especially for the first four weeks, with minimums on Saturday and maximums early in the week, on Sunday, Monday, or Tuesday. The pattern shifts forward a day or two in the last 2 1/2 weeks, when minimums are on Monday and Tuesday, and maximums around Wednesday and Thursday. The first day in Figure 11-16 is Friday, and the days are labeled every 7 days, i.e., July 20, July 27, etc.

The second EOF explaining 22.6% of the gradient has the strongest gradient in a strip running north-south through the entire length of the state and just west of the urban corridor. This pattern is also suggestive of urban sources. In this case, the associated meteorology is probably predominantly westerly winds, similar to the conditions for sulfur EOF 2.

The third and fourth EOFs for OMH, explain 11.8 and 9.2% of the variance, respectively. They also show strong gradients around single monitoring sites, North Bend on EOF 3 and Puyallup on EOF 4.

The time factors show that EOF 3 is weighted highest on August 10 and 23. The two highest OMH concentrations at North Bend, 19.4 and 17.8 $\mu g/m^3$, respectively, were also on these days. August 10 also had the highest fine mass (22.9) and b_{abs} (3.6) concentrations measured for this site. On August 23 the fine mass concentration at North Bend was 14.3 $\mu g/m^3$ and b_{abs}, was 1.8 $\mu g/m^3$. Both these concentrations are about average for this site. It seems likely that there was a nearby fire on August 10. The cause of the relatively high OMH concentration on August 23 is less clear, but it may also have been due to a fire.

The EOF 4 pattern results from an unusually high OMH concentration of 30.5 $\mu g/m^3$ at Puyallup on a single day, August 27. The next highest OMH concentration at any site was 19.4 $\mu g/m^3$. The concentration, though high, appears to be real. The fine mass concentration at the same site on this day was 32 $\mu g/m^3$ (highest fine mass concentration anywhere during the study was 35.2) and the b_{abs} concentration was 8 $\mu g/m^3$ (highest anywhere during the study). The pattern shown in EOF 4 is probably the result of a nearby fire.

11.5.4 b_{abs}

The contour plot of mean fine b_{abs} is shown in Figure 11-17. The highest mean concentration was 2.2 $\mu g/m^3$ measured at Puyallup. Three other sites, North Bend, Kent, and Sultan also had mean concentrations greater than 1.5 $\mu g/m^3$. Packwood, near the southeastern corner of the network had a mean concentration of 1.3 $\mu g/m^3$, which is higher than the other sites nearby. Mean b_{abs} concentrations at the receptor sites were 1.1, 0.8, and 0.9 $\mu g/m^3$, at Tahoma Woods, Paradise, and Marblemount, respectively.

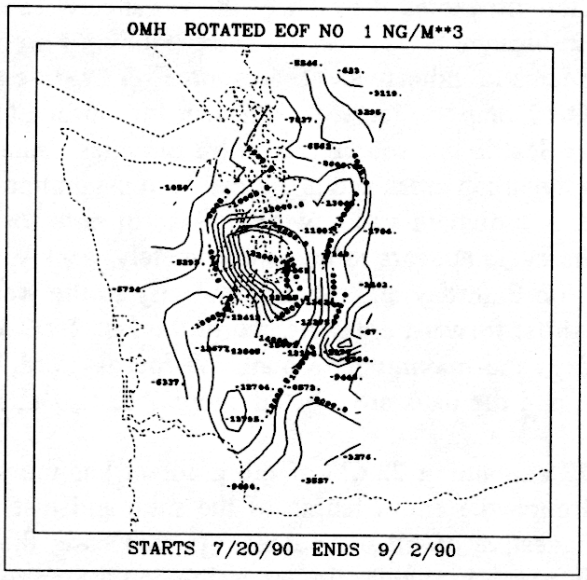

Figure 11-12. Rotated EOF 1 for OMH explaining 38.7% of the variance.

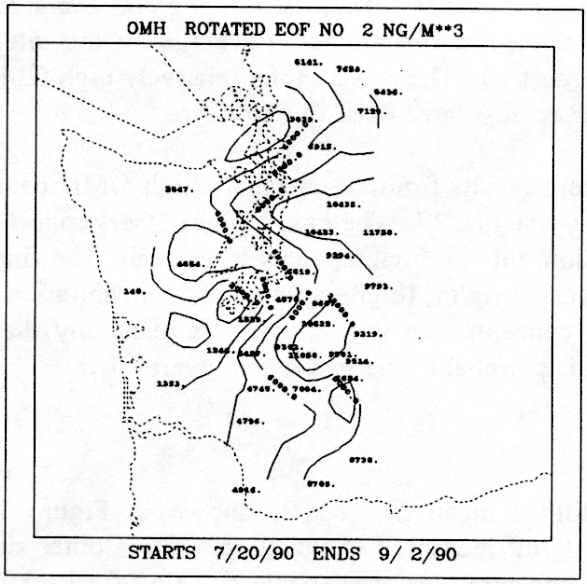

Figure 11-13. Rotated OMH EOF 2 explaining 22.6% of the variance. Contour interval is 2000 ng/m^3.

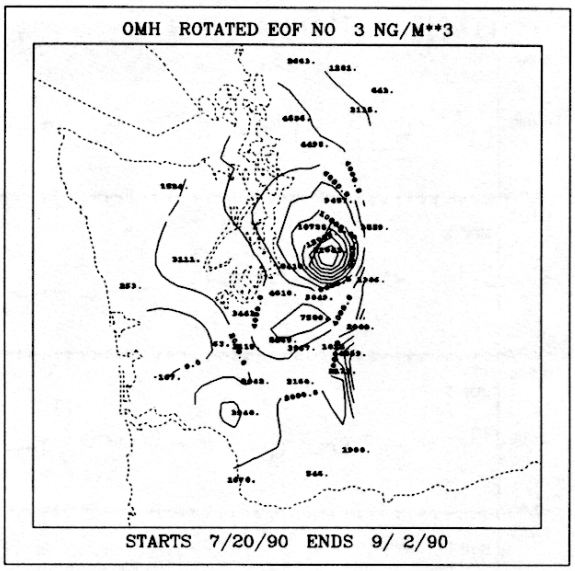

Figure 11-14. Rotated OMH EOF 3 explaining 11.8% of the variance. Contour interval is 2000 ng/m^3.

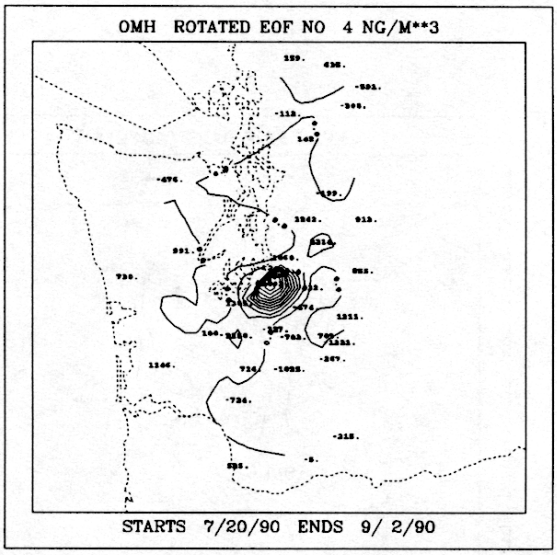

Figure 11-15. Rotated OMH EOF 4 explaining 9.2% of the variance. Contour interval is 2000 ng/m^3.

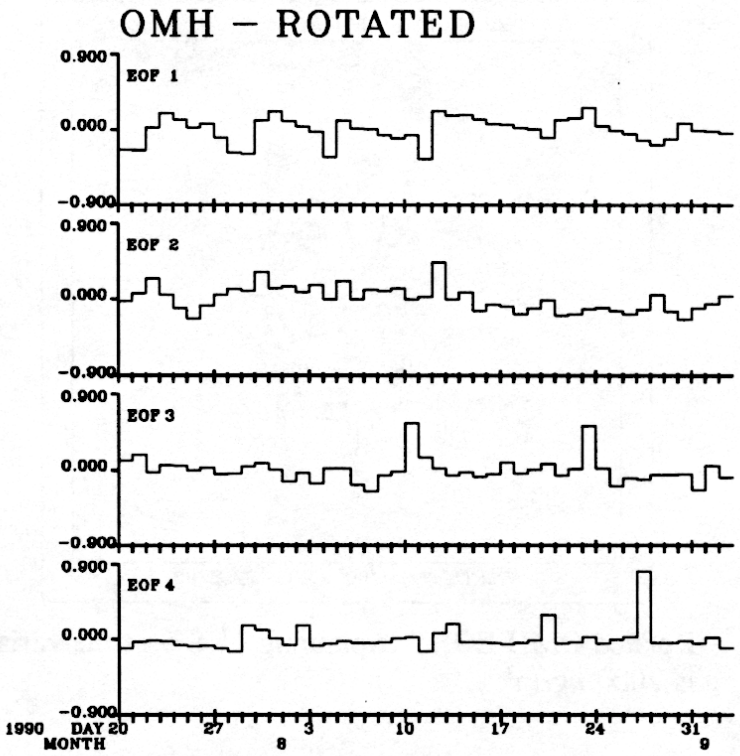

Figure 11-16. Time factors for first four rotated EOFs for OMH.

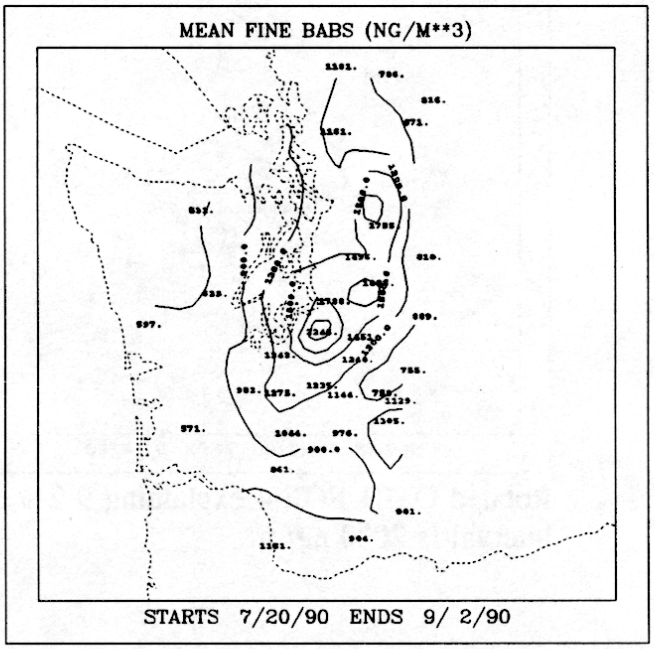

Figure 11-17. Contour plot of mean fine b_{abs}. Contour interval is 300 ng/m^3.

The time plots of b_{abs} at the receptor sites are shown in Figure 11-18. The highest concentration at Tahoma Woods was 2.3 $\mu g/m^3$ on August 11. This was part of a 5-day episode from August 7-11 when the 24-hour average b_{abs} concentration remained greater than 1.9 $\mu g/m^3$. Another three-day episode of concentrations from 1.6 to 2.0 $\mu g/m^3$ occurred August 2-4. Additionally, concentrations on July 20 and 21 were 1.9 and 1.8 $\mu g/m^3$ and on July 28 and 29 were 1.7 and 1.8 $\mu g/m^3$, respectively, and on August 28 the concentration was 2.0 $\mu g/m^3$. The highest value at Paradise was 1.5 $\mu g/m^3$ on August 28. Other days with relatively high concentrations at Paradise coincided roughly with the highest concentration days at Tahoma Woods. The highest concentration at Marblemount was 1.6 $\mu g/m^3$ on August 3. Other days with concentrations greater than 1.2 $\mu g/m^3$ at Marblemount included July 22-23, July 30-31, August 9, and August 14.

Six b_{abs} EOFs, accounting for a total of 86.8% of the variance were retained for Varimax rotation. Contour plots of the first four are shown in Figures 11-19 through 11-22, and the corresponding time factors are shown in Figure 11-23. EOF 1 for b_{abs}, which accounts for 27.3% of the variance shows several areas of strong gradients, the strongest is around Puyallup, with others around Rochester and Sultan and in the southwestern corner of the network near Ohanapacosh and Packwood. This pattern suggests that b_{abs} concentrations may often be due to several localized sources throughout the network. Slash and control burns are one possibility. The second EOF, accounting for 21.4% of the variance shows a gradient centered around Kent. This pattern was weighted the strongest on August 11, when the b_{abs} concentration was the second highest measured at Kent.

EOFs 3 and 4, which account for 12.5 and 12.1% of the variance, respectively, are indicative of urban sources, though this interpretation is not as clear as were EOFs 1 and 2 for sulfur and OMH. The strongest gradients on EOF 4, for example appear to radiate outward from the Seattle area, but are somewhat far north to implicate Tacoma. The apparent gradient around Packwood on EOF 3 may be an artifact of nine days of missing b_{abs} data at this site. A qualitative look at the time plots of b_{abs} at Packwood and other sites nearby, including Paradise, Ohanapacosh, and Glenoma show no obvious differences in the concentrations between these sites.

11.5.5 Sodium

The contour map of mean sodium concentrations is shown in Figure 11-24. The pattern is close to what might be expected if the sodium concentrations are primarily related to sea salt. Concentrations generally are lower inland than they are near the coast. The exception to this is the mean concentration at Skookumchuck which is higher than any of the sites around it. The high mean value at Skookumchuck is due to a high concentration (523 ng/m^3) on one day, which was the highest sodium concentration measured during the analysis period. In order to confirm or deny the validity of this concentration, the ground level trajectories for Skookumchuck and Rochester for this day were examined. Although the wind speeds were low, thus making the trajectory directions more uncertain than on days with higher wind speeds, the trajectories appear to be consistent with the concentrations. The trajectories arriving at Skookumchuck on August 11 passed over Puget Sound while air arriving at Rochester arrived from inland.

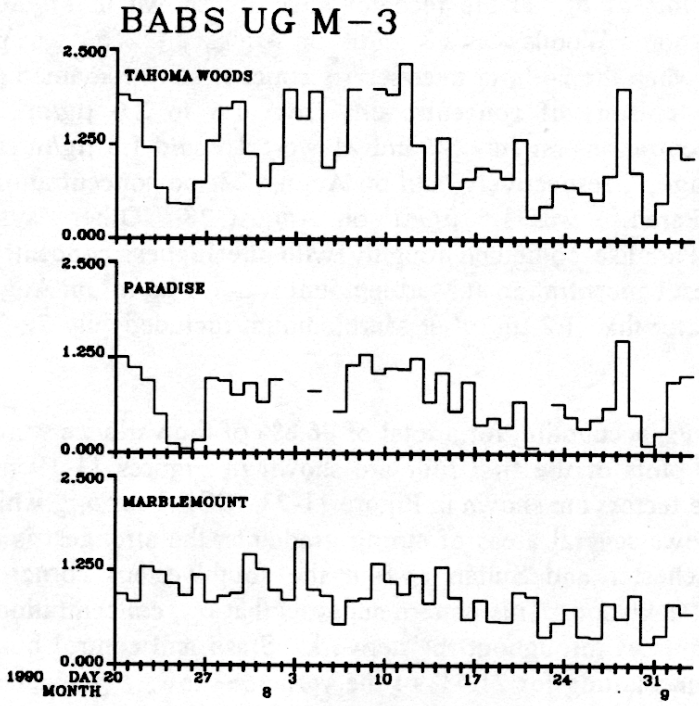

Figure 11-18. Time line of b_{abs} at the three receptor sites.

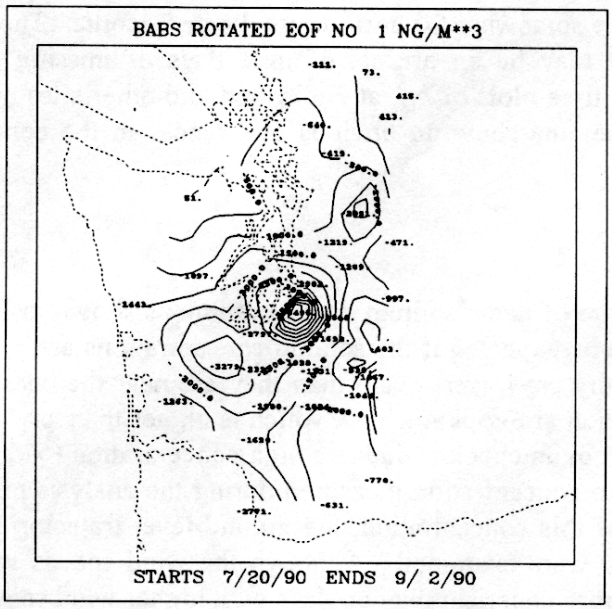

Figure 11-19. Rotated EOF 1 for b_{abs} explaining 27.3% of the variance. Contour interval is 500 ng/m^3.

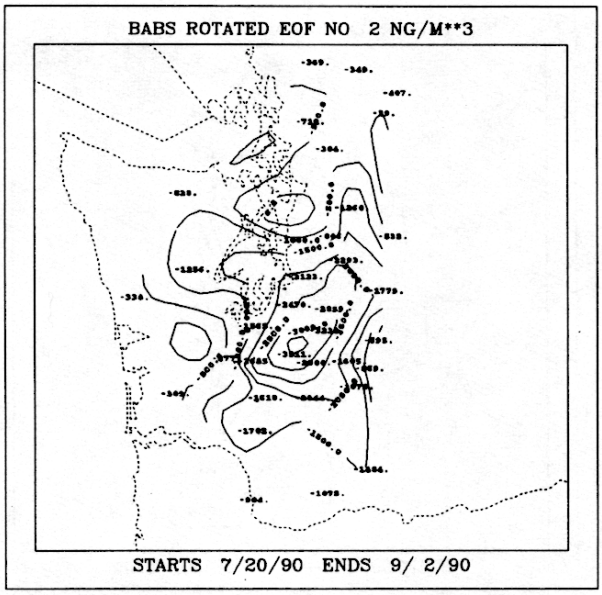

Figure 11-20. Rotated EOF 2 for b_{abs} explaining 21.4% of the variance. Contour interval is 500 ng/m^3.

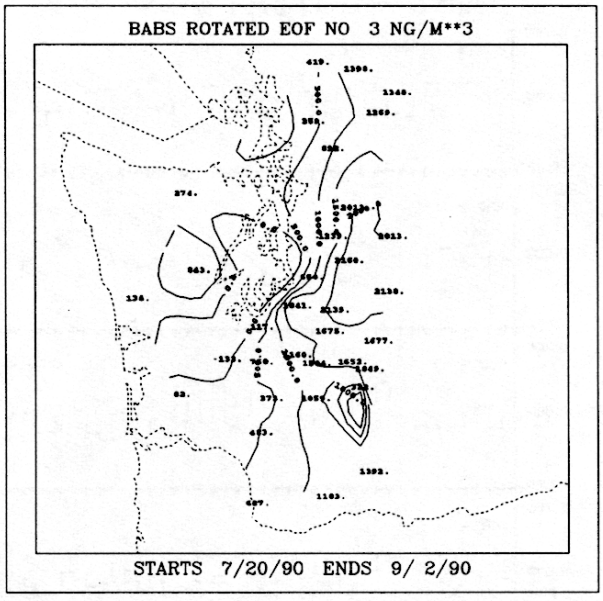

Figure 11-21. Rotated EOF 3 for b_{abs} explaining 12.5% of the variance. Contour interval is 500 ng/m^3.

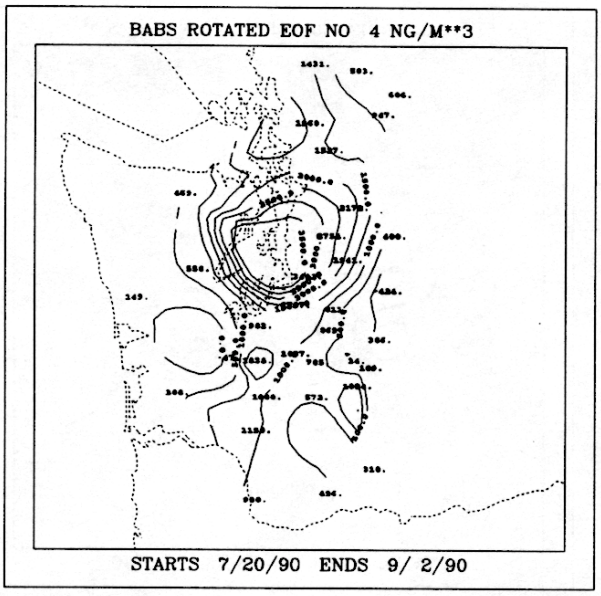

Figure 11-22. Rotated EOF 4 for b_{abs} explaining 12.1% of the variance. Contour interval is 500 ng/m^3.

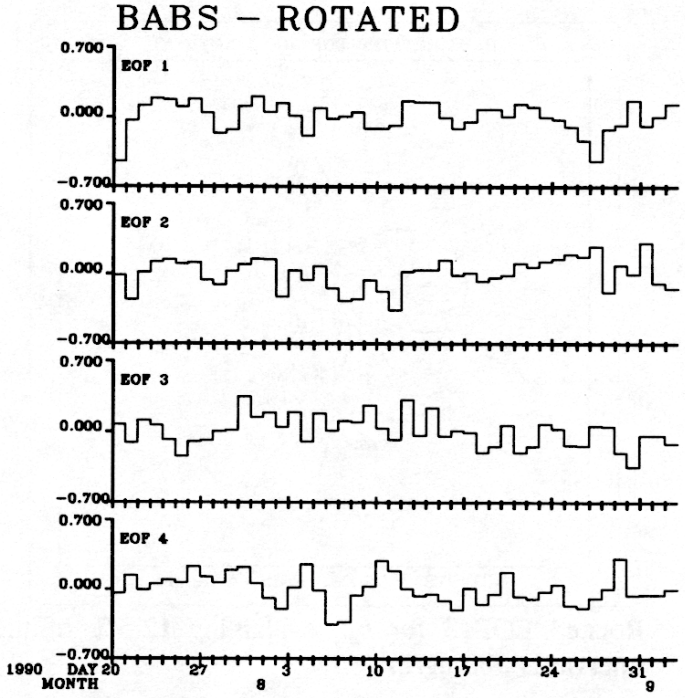

Figure 11-23. Time factors for the first four rotated EOFs for b_{abs}.

The highest mean sodium concentration was 158 ng/m^3 at Humptulips. The mean concentrations at the receptor sites were 37, 27, and 31 ng/m^3 at Tahoma Woods, Paradise and Marblemount, respectively.

Time lines of the sodium concentrations at the receptor sites are shown in Figure 11-25. The highest concentration was 117 ng/m^3 at Marblemount on July 23. The highest concentration at Tahoma Woods was 102 ng/m^3 on the same day. The highest value at Paradise was lower, as might be expected due to the higher elevation there, 77 ng/m^3, on August 8.

Six EOFs, explaining a total of 85.4% of the variance were rotated for sodium. The maps of the first three EOFs are shown in Figures 11-26 through 11-28, and the associated time factors are in Figure 11-29. The first EOF, explaining 25.4% of the variance, has the strongest gradient along the coast, consistent with what would be expected for transport of sea salt inland from the Pacific Coast. The second EOF, explaining 14.2% of the variance, has a strong gradient around Skookumchuck. This is partly due to the high concentration there on August 11, as discussed previously. However, the time factors indicate that other days, especially in the first half of the study period also loaded onto EOF 2. The third EOF, explaining 13.1% of the variance has the highest gradients surrounding Puget Sound. This is also consistent with a marine source of sodium.

11.5.6 Bromine

The highest bromine concentration measured was 32.5 ng/m^3 at Sultan on July 28. This value is more than a factor of five greater than the next highest concentration. It may or may not be real, but if left in the analysis, it is extremely influential in determining the spatial patterns of both the mean concentrations and the EOFs. Although EOF analysis was performed for bromine with this data point both in and out, only the results with it removed are presented. This gives a better picture of the overall patterns in the bromine concentrations which occurred during the study.

The map of mean bromine concentrations (with the 32.5 value at Sultan removed) is shown in Figure 11-30. Bromine is often considered to be a tracer for automobile exhaust and/or refineries (See Chapter 9). The spatial pattern shown in Figure 11-30 is consistent with an automobile (urban) source for bromine. The highest mean concentration was 2.88 ng/m^3 at Puyallup.

A time plot of the bromine concentrations at the receptor sites is shown in Figure 11-31. Qualitatively, concentrations at Tahoma Woods and Paradise seem to show similar temporal patterns, with both sites having several periods of gradually falling and rising concentrations. Averages for each day of the week were calculated for all three receptor sites. The highest mean concentrations at both Mount Rainier sites were on Saturdays, second highest on Sundays and lowest on Tuesdays. (The first day on the graph is Friday). This pattern was not seen in the bromine concentrations at Marblemount in North Cascades National Park.

The highest average concentration there was on Thursday and lowest on Saturday. The average concentrations for each day of the week for the receptor sites are shown in Table 11-2.

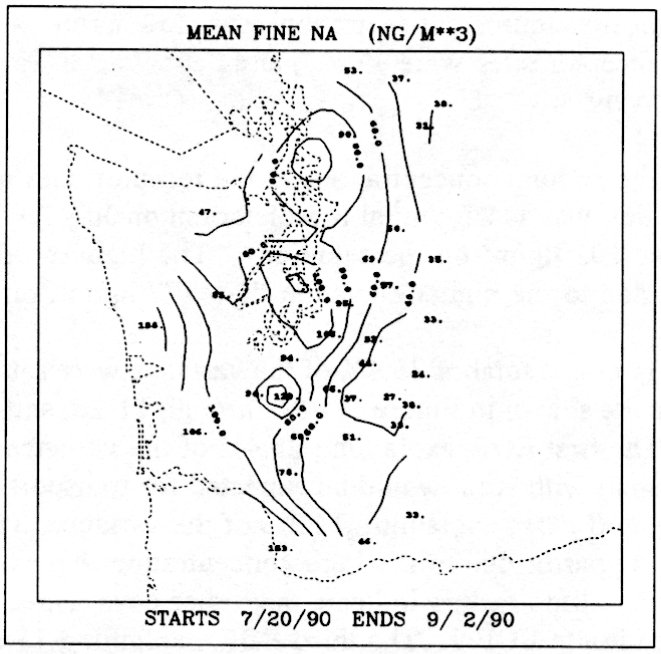

Figure 11-24. Contour plot of mean fine sodium. Contour interval is 20 ng/m^3.

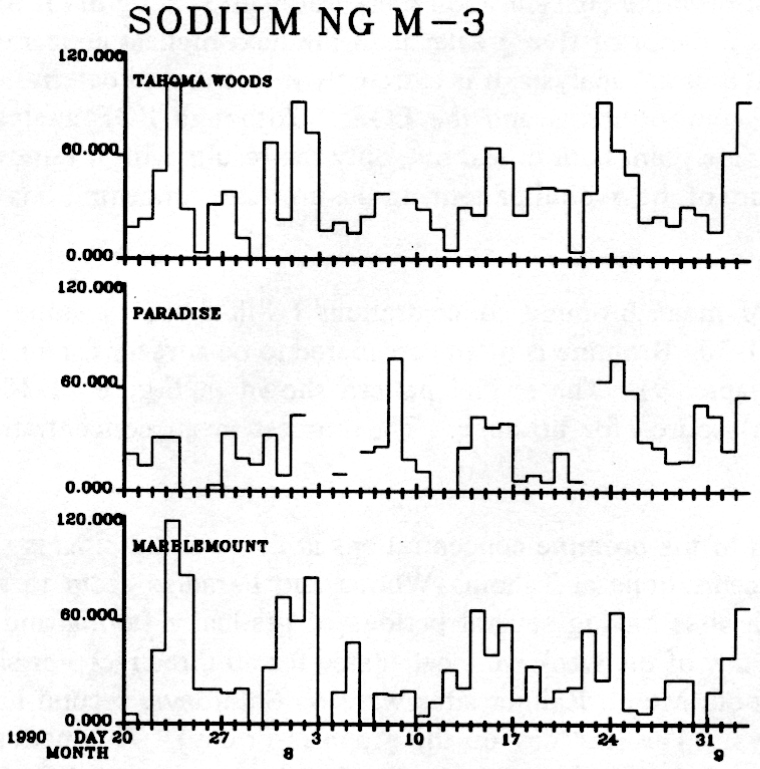

Figure 11-25. Time lines of sodium at the receptor sites.

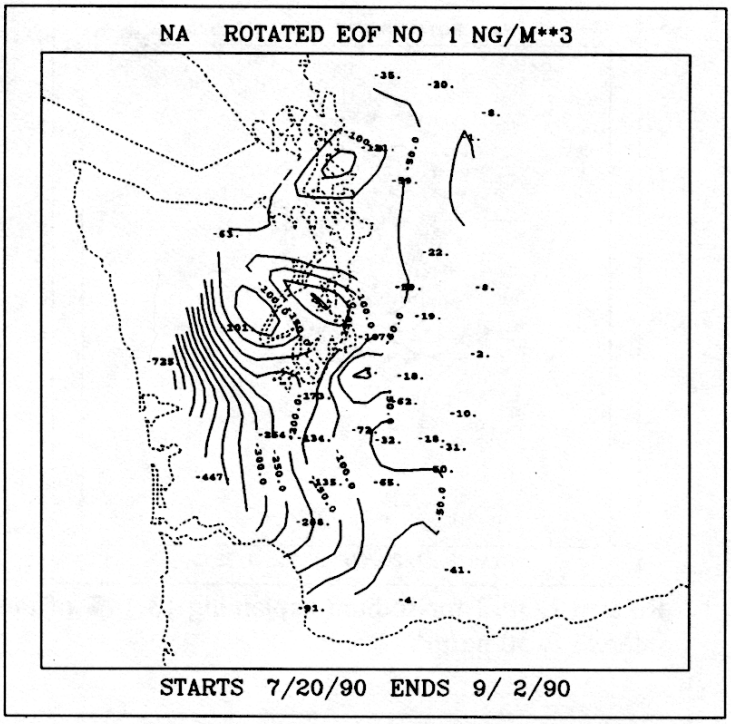

Figure 11-26. EOF 1 for sodium explaining 24.5% of the variance. Contour interval is 50 ng/m^3.

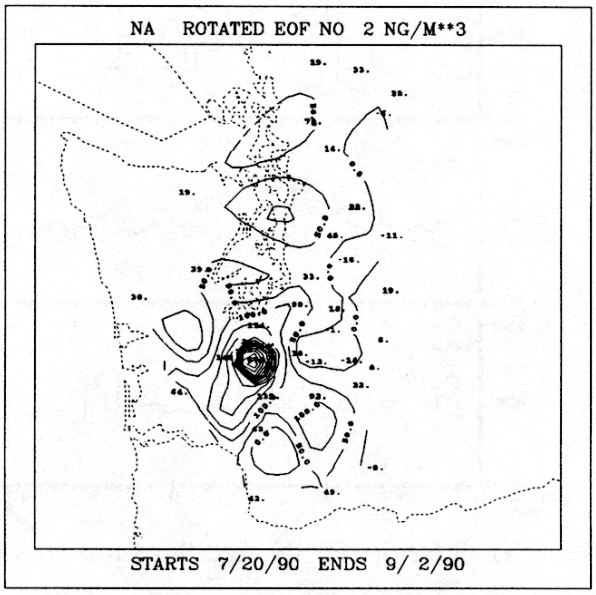

Figure 11-27. Rotated EOF 2 for sodium explaining 14.2% of the variance. Contour interval is 50 ng/m^3.

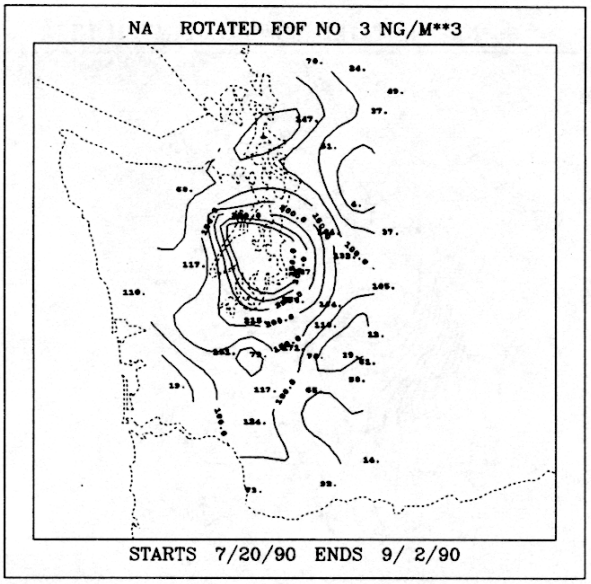

Figure 11-28. Rotated EOF 3 for sodium explaining 13.1 % of the variance. Contour interval is 50 ng/m^3.

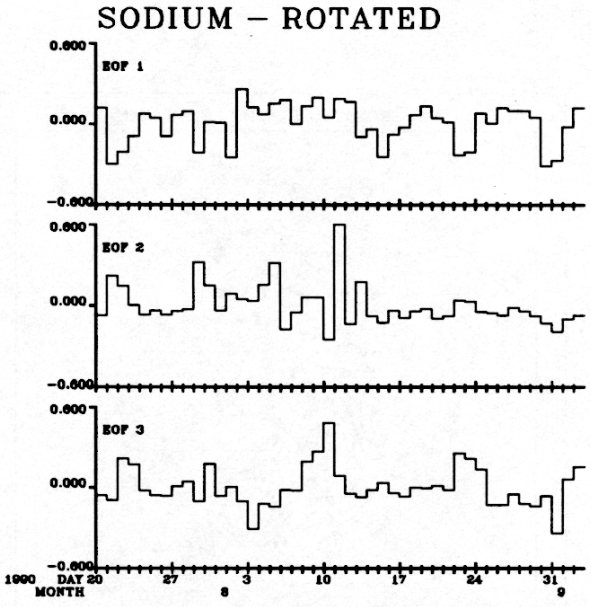

Figure 11-29. Time factors for the first three rotated sodium EOFs.

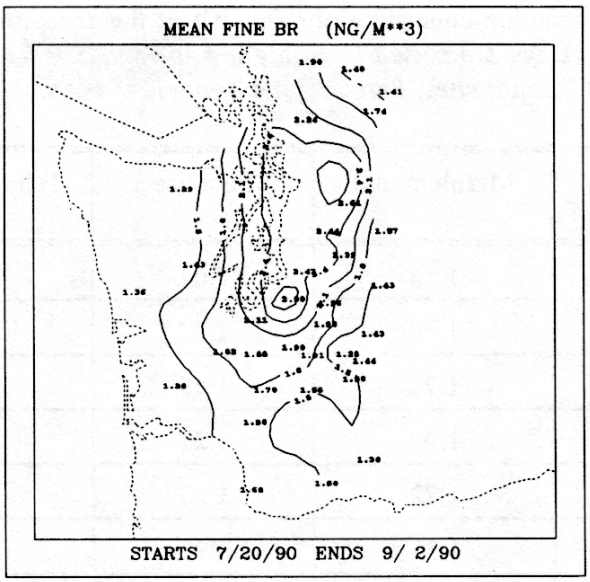

Figure 11-30. Contour plot of mean bromine concentrations with the high value on July 28 at Sultan removed. Contour interval is 0.3 ng/m^3.

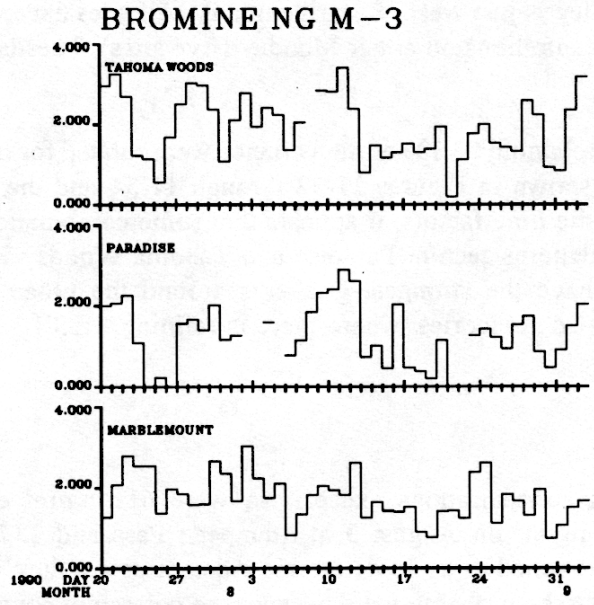

Figure 11-31. Bromine concentrations at the three receptor sites.

Table 11-2. Mean bromine concentrations (ng/m^3) at the receptor sites for each day of the week. Days are sorted from highest to lowest mean concentrations at the two Mount Rainier sites, Paradise and Tahoma Woods.

Day of the Week	Marblemount	Paradise	Tahoma Woods
Saturday	1.53	1.61	2.46
Sunday	1.90	1.57	2.31
Friday	1.77	1.45	2.07
Thursday	1.92	1.21	1.86
Monday	1.72	1.20	1.49
Wednesday	1.57	0.92	1.42
Tuesday	1.76	0.84	1.40

Similar daily averages calculated for all sites show that 31 of the 34 sites have highest daily average bromine concentrations on either Saturday or Sunday. The only exceptions are Marblemount as discussed previously; and Sauvie Island and Sedro Woolley which both have maximum daily averages on Friday. Sauvie Island is near Portland on the south end of the network, Sedro Woolley is just west of Marblemount. All sites except Marblemount had lowest average bromine concentrations on either Monday (five sites), Tuesday (20 sites) or Wednesday (eight sites).

Four EOFs, explaining 83.1% of the variance were rotated for bromine. The contour plots of the first three are shown in Figures 11-32 through 11-34 and the time factors are shown in Figure 11-35. From the time factors, it appears that some combination of EOFs 1 and 2 would generate the weekly patterns seen at Paradise and Tahoma Woods. EOFs 1 and 2 are spatially similar, also. Both have the strongest gradients around the urban areas, including not only Seattle-Tacoma, but also Anacortes, where there is refining. EOF 3 has a very strong gradient around Puyallup.

11.5.7 Potassium

All potassium concentrations except two were 611 ng/m^3 or less. The two highest concentrations, 3529 ng/m^3 on August 3 at Stampede Pass and 1371 ng/m^3 on August 17 at Sauvie Island were examined to try to determine whether or not they were valid data. The 1379 value was determined to be probably valid because the potassium concentrations at 23 other sites were also higher than usual on the same day. This indicates that there was some physical reason for the high concentration. However, it was more difficult to determine the validity of the highest concentration. Potassium is usually thought to be from soil dust or fires. Therefore, iron (an indicator of soil), OMH, b_{abs}, and fine mass at Stampede Pass on August 3 were examined to see if any of these concentrations were also high. All of them were relatively low. This

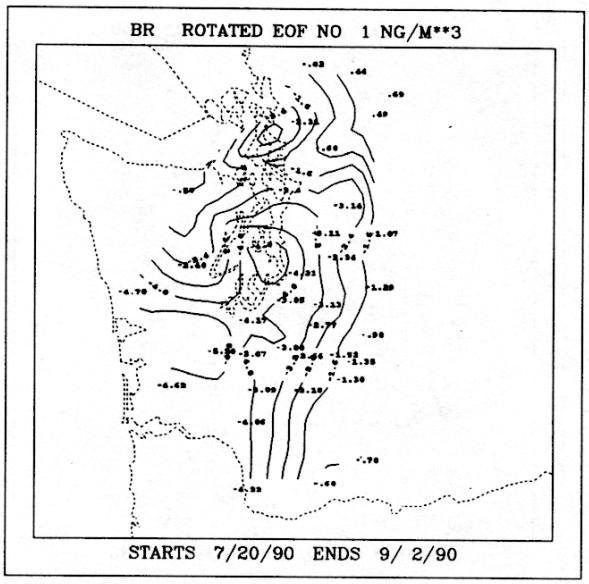

Figure 11-32. Rotated EOF 1 for bromine explaining 27.1% of the variance. Contour interval is 0.8 ng/m^3.

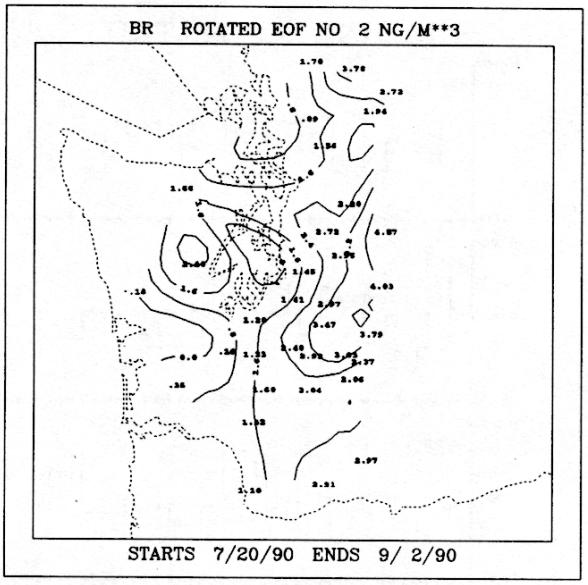

Figure 11-33. Rotated EOF 2 for bromine explaining 20.3% of the variance. Contour interval is 0.8 ng/m^3.

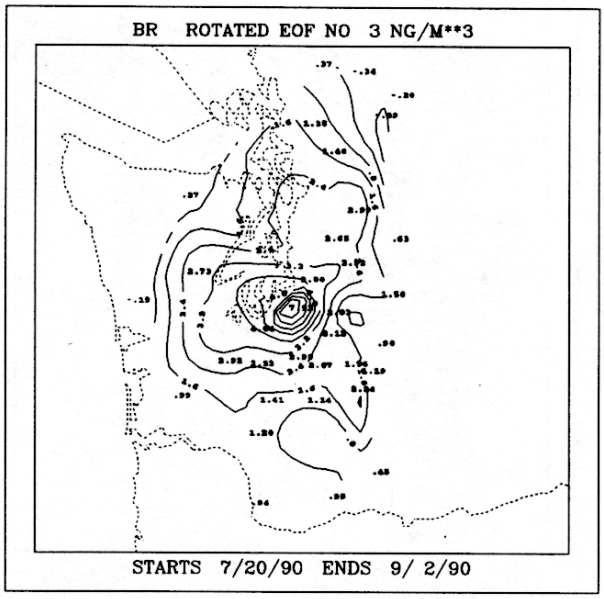

Figure 11-34. Rotated EOF 3 for bromine explaining 17.1% of the variance. Contour interval is 0.8 ng/m^3.

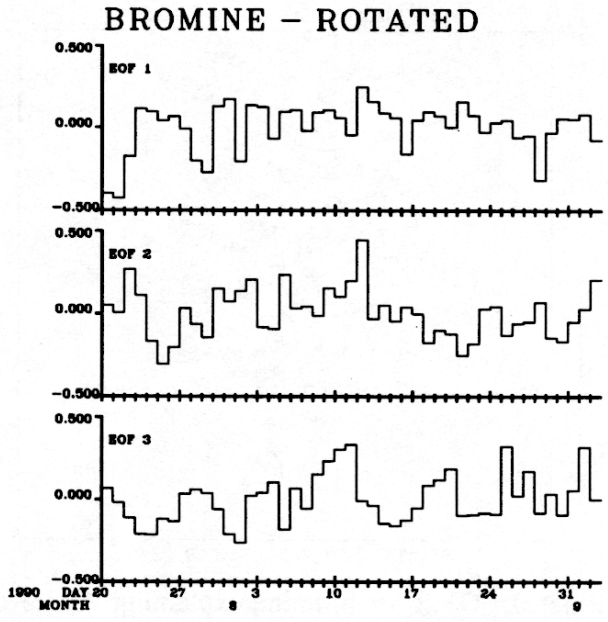

Figure 11-35. Time factors for rotated bromine EOFs.

seemed to rule out the existence of a nearby fire or higher than usual blowing soil concentrations as being the source of high potassium. However, these concentrations were also relatively low at Sauvie Island on August 17, so this did not seem like sufficient reason to eliminate the data point.

EOF analyses were conducted with this concentration both included and deleted. When the value is included, it loads exclusively onto rotated EOF 1 and the spatial patterns associated with the remaining EOFs are not much different than if it is removed. Therefore, only the results with this concentration included are presented.

A contour plot of the mean potassium concentrations is shown in Figure 11-36. It is unusual compared to the other species examined so far, in that the highest mean value, 155 ng/m^3, is at Sauvie Island on the southern edge of the PREVENT network. Even if the high value measured on August 17 is removed, Sauvie Island still has the highest mean concentration (127 ng/m^3). The next highest concentration is 122 ng/m^3 at Stampede Pass. However, without the high value on August 3, the average at Stampede Pass is only 49 ng/m^3. The next highest mean concentrations are in the center of the network at Puyallup (98 ng/m^3), Skookumchuck (95 ng/m^3) and North Bend (90 ng/m^3). Sauvie Island is near Portland, Oregon.

A time plot of the potassium concentrations at the receptor sites is shown in Figure 11-37. Each of the three sites have one or two days when the concentration was much higher than on the rest of the days. These days are August 17 at Tahoma Woods, August 16 at Paradise, and July 23 and August 17 at Marblemount.

Clearly, something interesting happened on August 17. The wind directions at 3000 and 6000 ft. on this day were mostly southerly and southwesterly with moderately high wind speeds. So, it appears, that potassium was transported into western Washington from Oregon. The source type associated with the high potassium concentrations is less clear, however. Other indicators of fires: fine mass, OMH, and b_{abs} were not particularly high across the PREVENT network on this day and neither were iron concentrations which would indicate blowing dust.

Six EOFs, explaining 97.4% of the variance were rotated for potassium. The first four are shown in Figures 11-38 through 11-41 and the time factors are shown in Figure 11-42. As discussed above, the first EOF is associated nearly exclusively with the high concentration at Stampede Pass on August 3. EOFs 2, 3, and 5 (5 is not shown) all appear to be indicative of transport of potassium into the region from the southwest, and EOF 4 indicates transport from the southeast. EOF 2 also has a relatively strong gradient around Carbon River and Mud Mountain.

11.5.8 Manganese

The highest manganese concentration was 35 ng/m^3 at Kent on August 28. All other concentrations were 15 ng/m^3 or less. The concentrations of several other species were also high at Kent on this day, including b_{abs}, fine mass, and OMH, so the high manganese concentration was assumed to be valid.

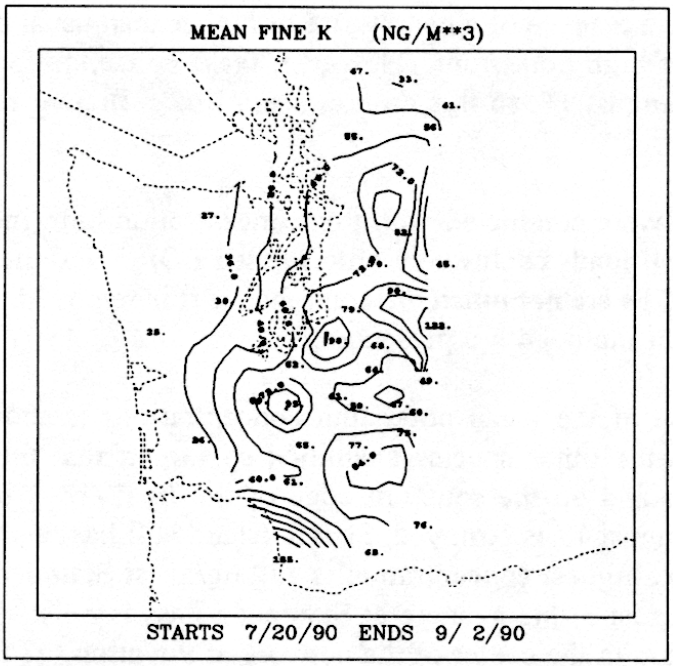

Figure 11-36. Mean potassium concentrations. Contour interval is 12 ng/m^3.

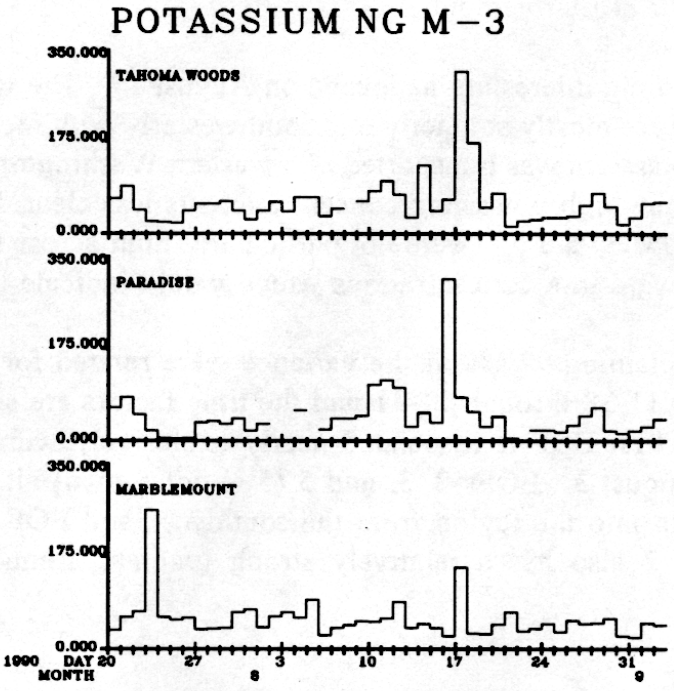

Figure 11-37. Potassium concentrations at the receptor sites.

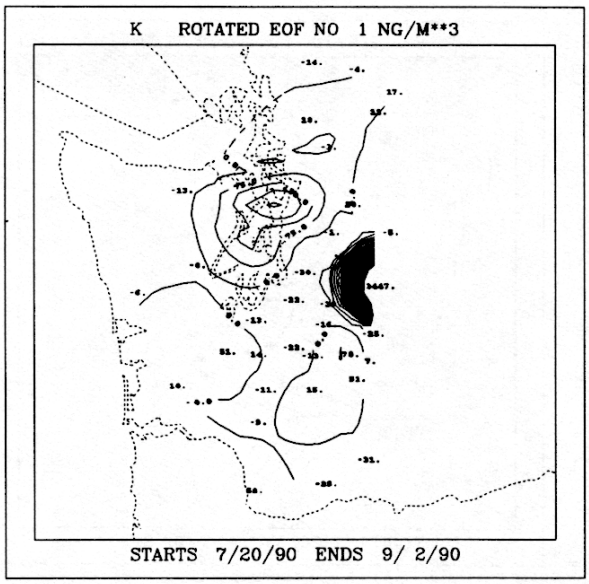

Figure 11-38. Rotated EOF 1 for potassium, explaining 68.3% of the variance. Contour interval is 75 ng/m^3.

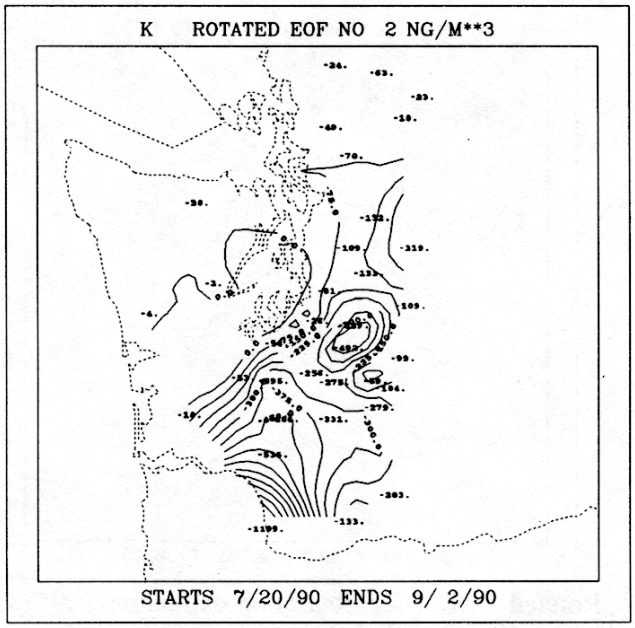

Figure 11-39. Rotated EOF 2 for potassium explaining 17.0% of the variance. Contour interval is 75 ng/m^3.

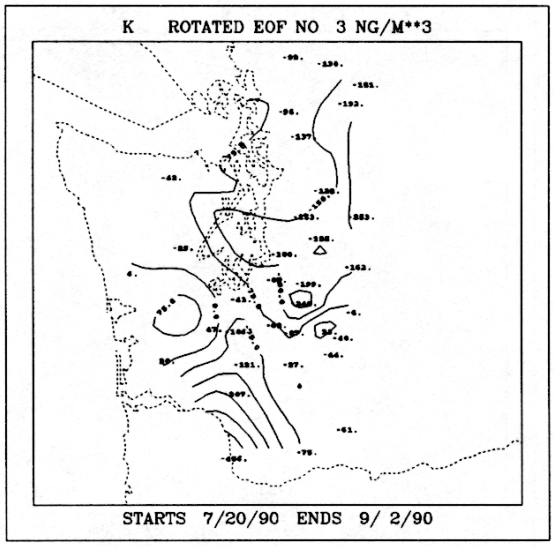

Figure 11-40. Rotated EOF 3 for potassium explaining 4.1% of the variance. Contour interval is 75 ng/m^3.

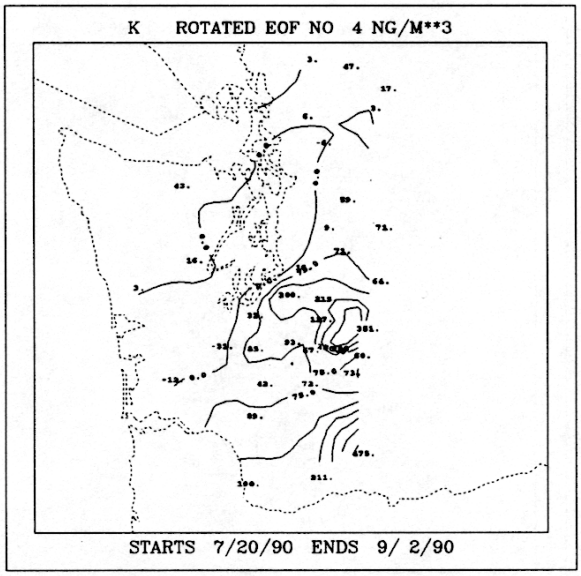

Figure 11-41. Rotated EOF 4 for potassium explaining 3.9% of the variance. Contour interval is 75 ng/m^3.

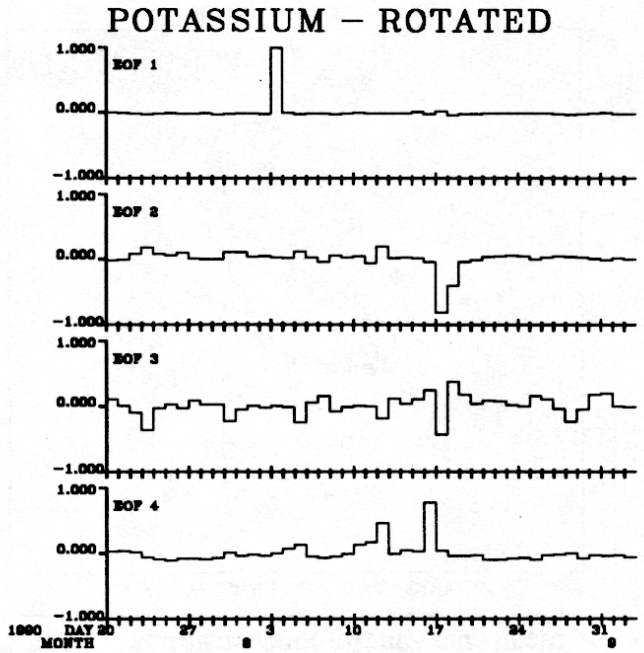

Figure 11-42. Time factors for the first four rotated EOFs for potassium.

The map of mean manganese concentrations is shown in Figure 11-43. The highest mean concentration is 6.1 ng/m^3 at Puyallup. Concentrations generally decrease outward from there, except they rise again to 2.5 ng/m^3 at Sauvie Island on the southern edge of the network near Portland and rise to 2.1 at Sedro Woolley and 2.7 at Kendall on the far northern edge of the network.

Time lines of the manganese measured at the receptor sites are shown in Figure 11-44. Although the concentrations at Tahoma Woods are usually greater than at Paradise, they appear to rise and fall together.

Seven EOFs explaining 89.4% of the variance were rotated for manganese. These are not shown, but only briefly described. The time factors for EOF 1 show that it was weighted very little for any day except August 28, and the map reflects the high concentration at Kent on this day. EOFs 2 and 6 have the strongest gradients around Puyallup, the site with the highest mean concentration. EOF 3, which was weighted most heavily during August 10-13, has the largest gradient around Skookumchuck, the site nearest the Centralia Power Plant. EOF 4 had only a weak gradient across the entire area, and EOF 5 showed a gradient around Sultan and North Bend.

11.5.9 Iron, Silicon, Aluminum, Titanium, Calcium

These elements are all associated with soil. The overall correlations between them, including data from all sites, are shown in Table 11-3. The correlations were all quite high ranging from 0.65 between calcium and aluminum to 0.95 between aluminum and silicon.

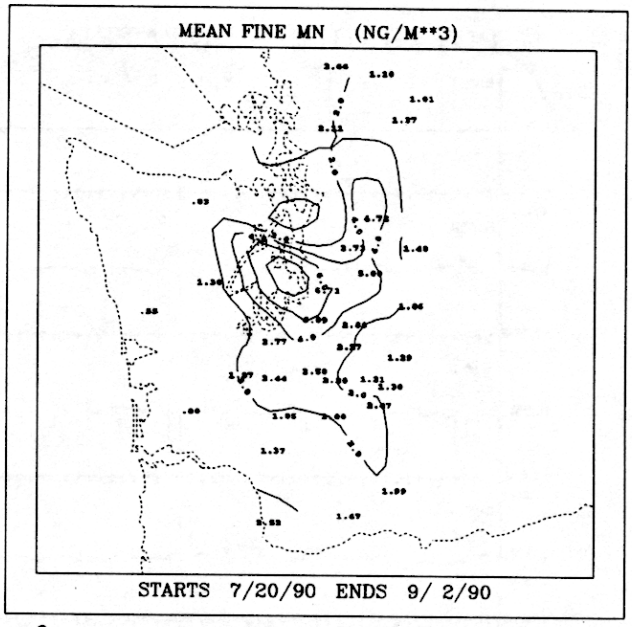

Figure 11-43. Map of mean manganese concentrations. Contour interval is 2 ng/m^3.

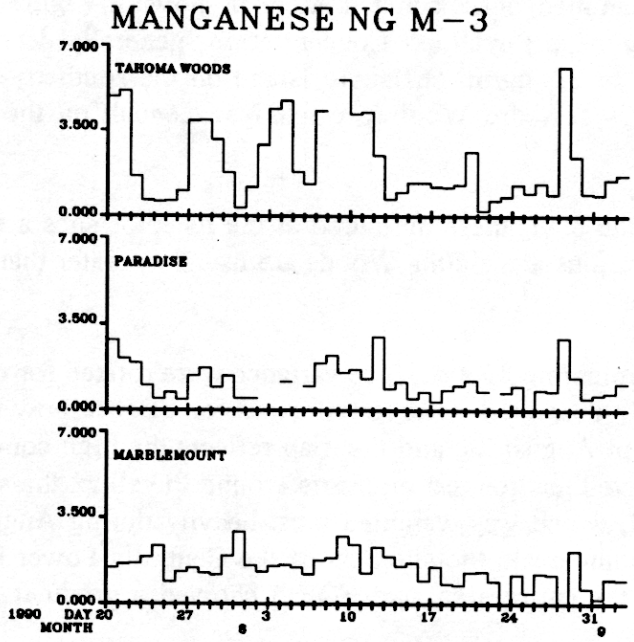

Figure 11-44. Manganese concentrations at the receptor sites.

Table 11-3. Correlations between elements usually considered to be associated with soil. Data from all 34 sites are included.

	Fe	Si	Al	Ca	Ti
Fe	1.00	0.93	0.84	0.88	0.93
Si	0.93	1.00	0.95	0.79	0.92
Al	0.84	0.95	1.00	0.64	0.87
Ca	0.88	0.79	0.64	1.00	0.78
Ti	0.93	0.92	0.87	0.78	1.00

Of these five elements, the highest mean concentrations were for silicon (39-428 ng/m^3), followed by iron (15-115 ng/m^3), aluminum (10-224 ng/m^3), calcium (9-61 ng/m^3), and titanium (2-12 ng/m^3).

The highest mean concentrations for all these elements were at Skookumchuck, the site nearest the Centralia Power Plant. This could indicate that these elements were associated not just with soil, but with emissions from the power plant. In fact some source profiles for coal-fired power plants which were used in the Chemical Mass Balance (CMB) model showed that these elements were all relatively high in the emissions from this source type (See Chapter 9).

The site with the second highest mean concentrations for all species was Sultan. Sultan is east and north of the Seattle-Tacoma urban area and south of North Cascades National Park. Unlike, some of the previously discussed elements, the mean soil element concentrations at these two sites were not high due to unusually high concentrations on one or two days. The values at these two sites are consistently higher than at the other sites on nearly every day. Trout Lake, in the far southwest corner of the network also has a mean concentration which is higher than the other sites near it.

Lowest mean concentrations were at the westernmost sites closest to the Pacific Coast including, Willapa, Humptulips, and Hurricane Ridge, and in the northeast corner at Newhalem and Mt. Baker Ski Area. A map of the mean iron concentrations is shown in Figure 11-45. The spatial patterns of the means of the other four elements were all very similar. Iron is shown because it had the fewest observations below MDL.

Time lines of the iron concentrations at the receptor sites are shown in Figure 11-46. The highest concentrations at Tahoma Woods and Paradise were on July 20 and 21 (82-86 ng/m^3) and again during August 9-11 at Tahoma Woods (62-100 ng/m^3) and August 10-12 at Paradise (66-79 ng/m^3). The highest concentrations at Marblemount were on August 9, 10, and 12 (67-69 ng/m^3) and on July 23 (64 ng/m^3). After August 17, iron concentrations remained less than 25 ng/m^3 at all three sites, except for relatively high values at Tahoma Woods (47 ng/m^3) and Paradise (48 ng/m^3) on August 28.

Four EOFs, explaining a total of 89.2% of the variance were rotated for iron. The first three are shown in Figures 11-47 through 11-49 and the time factors are in Figure 11-50.

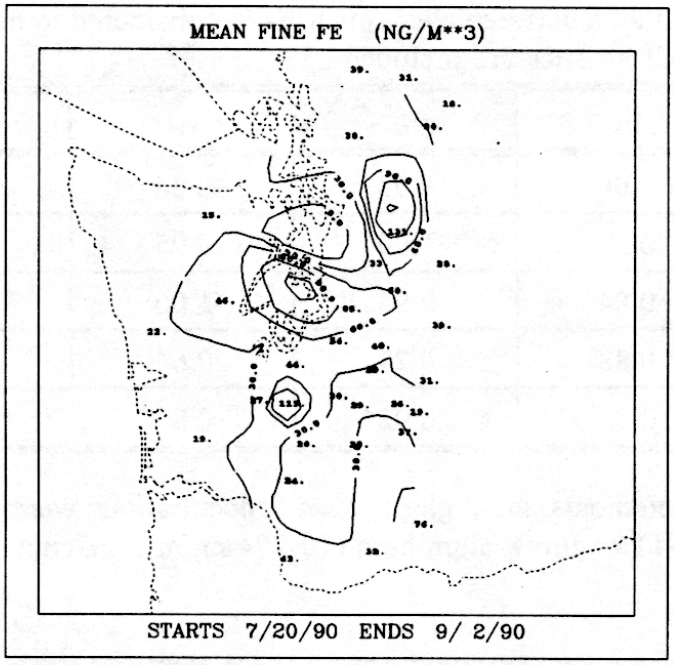

Figure 11-45. Map of mean iron concentrations. Contour interval is 30 ng/m^3.

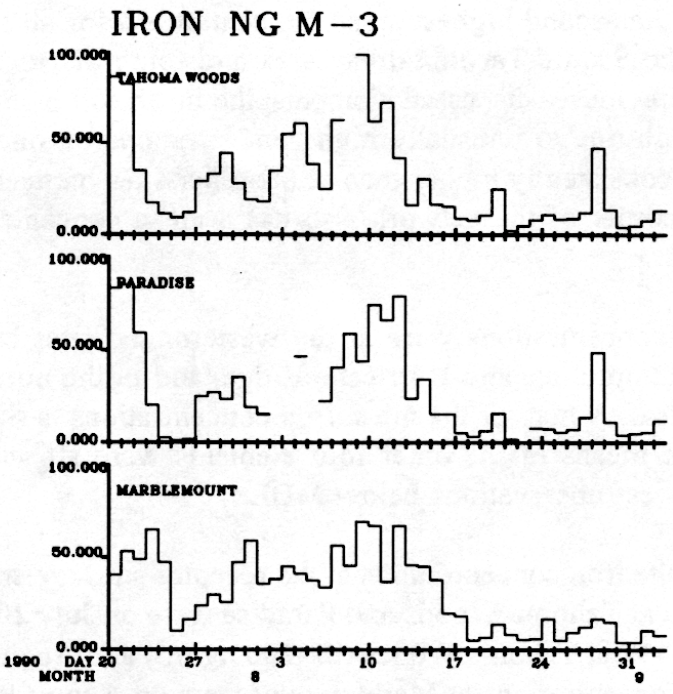

Figure 11-46. Iron concentrations at the receptor sites.

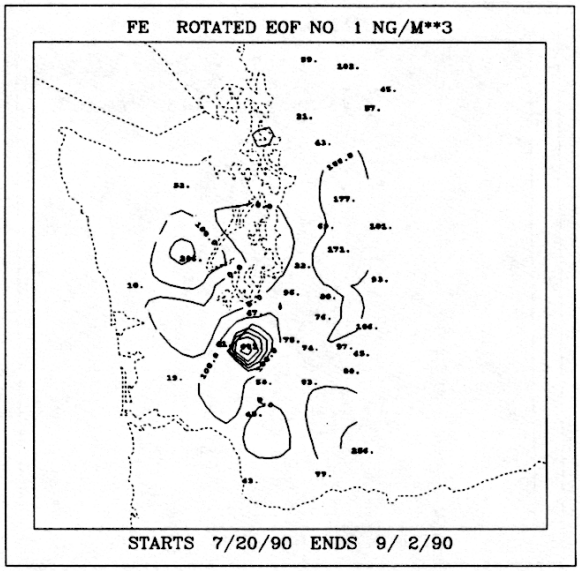

Figure 11-47. Rotated EOF 1 for iron explaining 31.0% of the variance. Contour interval is 100 ng/m^3.

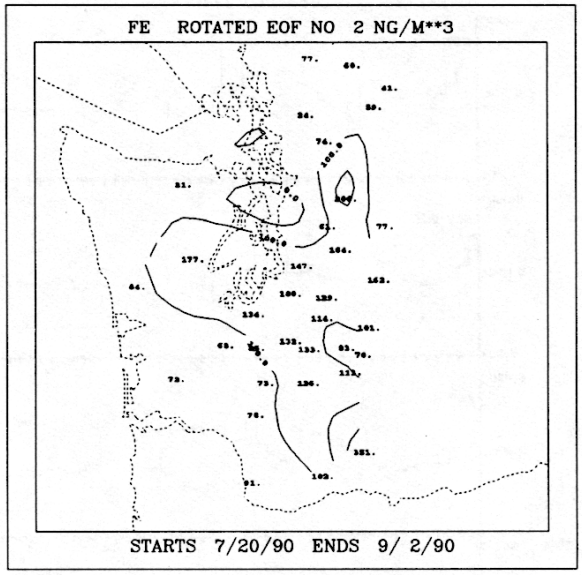

Figure 11-48. Rotated EOF 2 for iron explaining 22.7% of the variance. Contour interval is 100 ng/m^3.

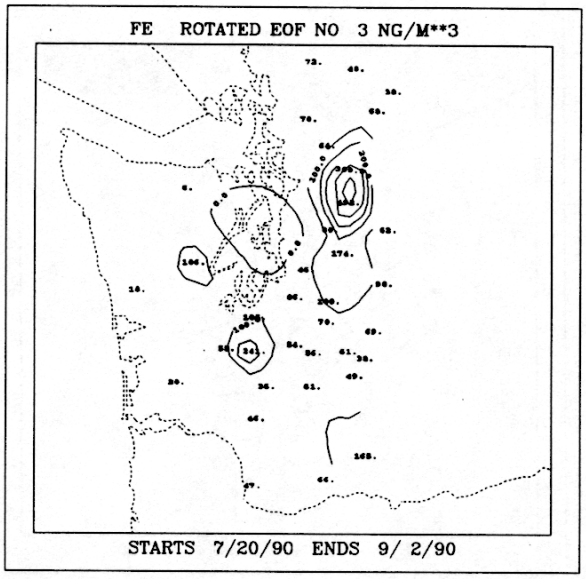

Figure 11-49. Rotated EOF 3 for iron explaining 21.0% of the variance. Contour interval is 100 ng/m^3.

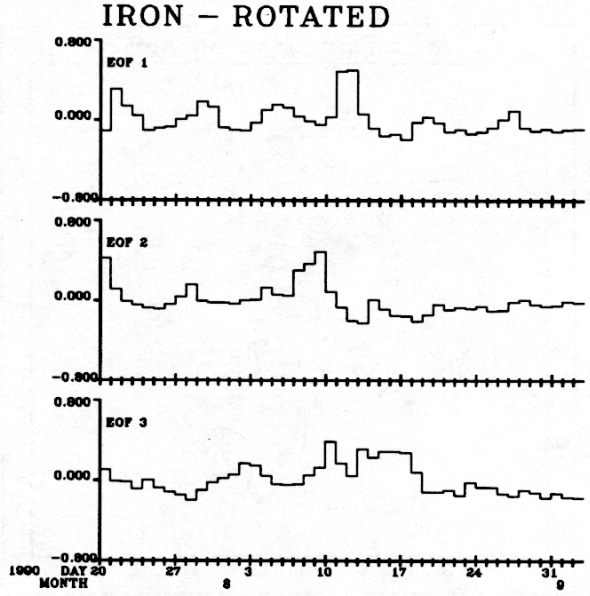

Figure 11-50. Time factors for first three rotated EOFs for iron.

The first EOF, explaining 31.0% of the variance, shows a strong gradient around Skookumchuck. The reasons for this are discussed previously. The second EOF, explaining 22.7% of the variance, shows mostly uniform values across the network but with small gradients around Trout Lake and Sultan. EOF 3, explaining 21.0% of the variance, shows a gradient around Sultan and slightly weaker gradients around Skookumchuck and Kent. All three EOFs show relatively high values at South Mountain also. The time factors indicate that the high iron episodes at Paradise and Tahoma Woods are associated with EOF 1 (July 21, August 11 and 12), EOF 2 (July 20 and August 9) and EOF 3 (August 10). The days with the highest iron concentrations at Marblemount load most strongly onto EOF 3.

The fourth EOF (not shown) has time weights which are significantly different than zero only on August 28 and the map shows a strong gradient around Kent. This is due to a high iron concentration (575 ng/m^3) at Kent on this day. This is the highest iron concentration measured during the analysis period, though it is not much higher than the next highest values (476, 414, 349, 329 ng/m^3, etc. in descending order). Also, concentrations of several other species, including, b_{abs}, fine mass, and OMH, were high at Kent on August 28, so there is no reason to believe that it is not valid.

11.5.10 Vanadium

A map of the mean vanadium concentrations is shown in Figure 11-51. The highest mean concentration was at Puyallup (3.3 ng/m^3). As with the soil elements, this was not due to 1 or 2 isolated high concentrations at this site, but was because the vanadium concentrations at Puyallup were consistently higher on a day-to-day basis than at the other sites. The second highest mean concentration was at Sedro Woolley (2.1 ng/m^3), which is the site nearest to Anacortes. The lowest mean vanadium concentrations were in the southeastern corner of the network.

Time plots of the vanadium concentrations measured at the receptor sites are shown in Figure 11-52. The percent of concentrations below the MDL (plotted as 0) at Tahoma Woods, Paradise, and Marblemount were 31, 36, and 24%, respectively. The average concentration at Tahoma Woods was 0.56 ng/m^3, which is more than double the mean concentration at Paradise (0.27 ng/m^3). The mean concentration at Marblemount was 0.52 ng/m^3.

The highest vanadium concentration measured at the receptor sites during the analysis period was 2.4 ng/m^3 at Marblemount on July 30. The highest concentrations at Tahoma Woods occurred during four episodes on July 29 (1.7 ng/m^3), August 3-5 (1.1-1.4 ng/m^3), August 9-11 (1.2-1.7 ng/m^3), and August 20 (1.8 ng/m^3).

Nine EOFs, explaining 87.1% of the variance were rotated for vanadium. The first four are shown in Figures 11-53 through 11-56 and the time factors are in Figure 11-57. EOF 1 has a strong gradient around Puyallup and weights mostly on August 27 when the highest concentration was measured there. EOFs 2 and 3 indicate stagnation around the Seattle-Tacoma urban area. Transport south from the Anacortes area is indicated in EOF 4. EOFs 6, 7, and 9 (not shown) all have some gradient around the Centralia area. This is seen to a lesser extent in EOF 2 also.

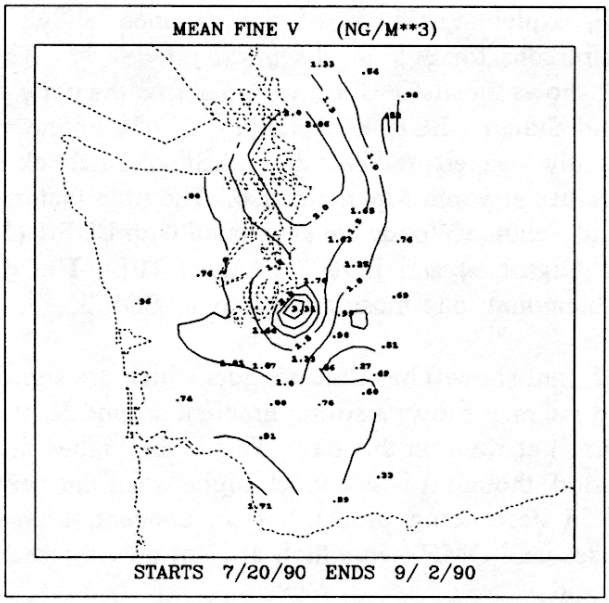

Figure 11-51. Map of mean vanadium concentrations. Contour interval is 0.5 ng/m^3.

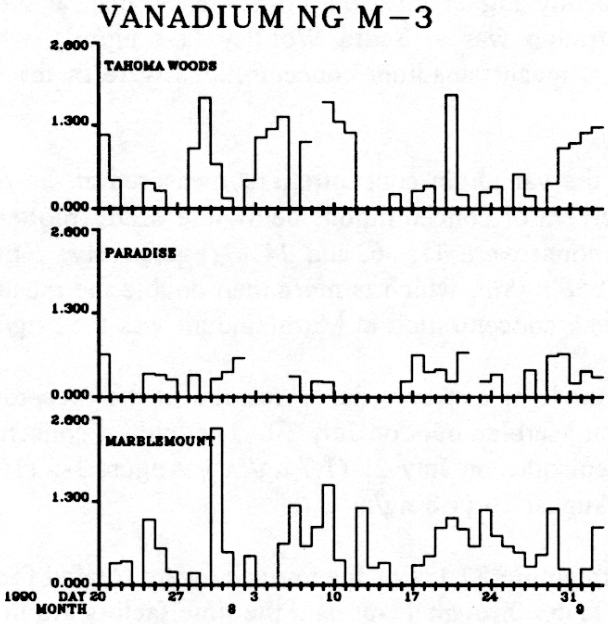

Figure 11-52. Time plot of vanadium concentrations at the receptor sites.

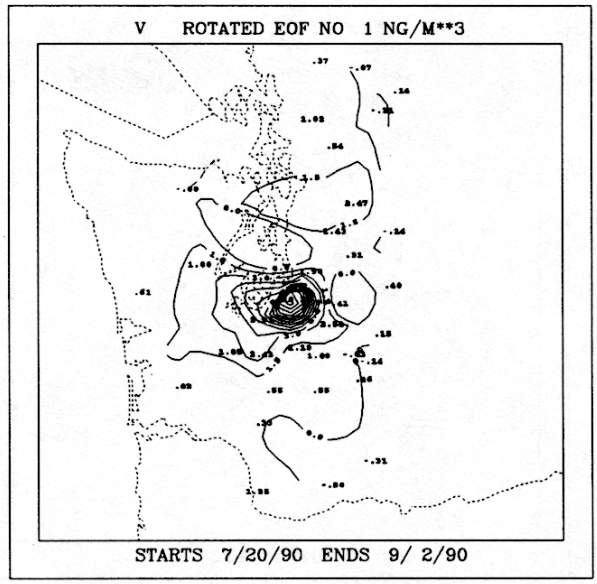

Figure 11-53. Rotated EOF 1 for vanadium explaining 34.9% of the variance. Contour interval is 1.5 ng/m^3.

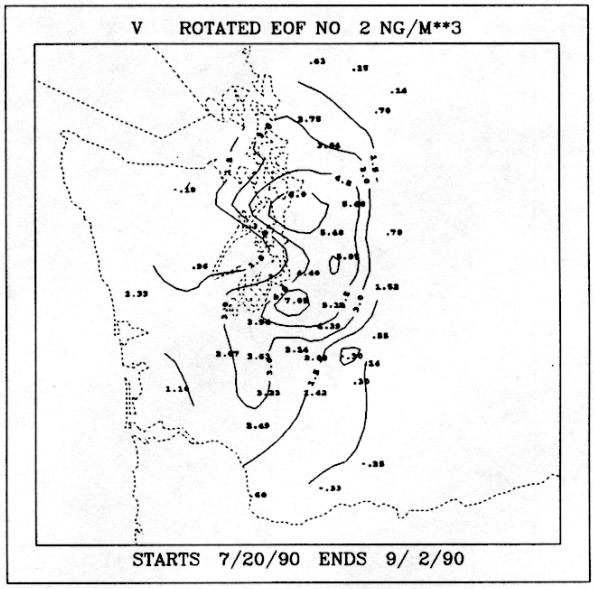

Figure 11-54. Rotated EOF 2 for vanadium explaining 21.3% of the variance. Contour interval is 1.5 ng/m^3.

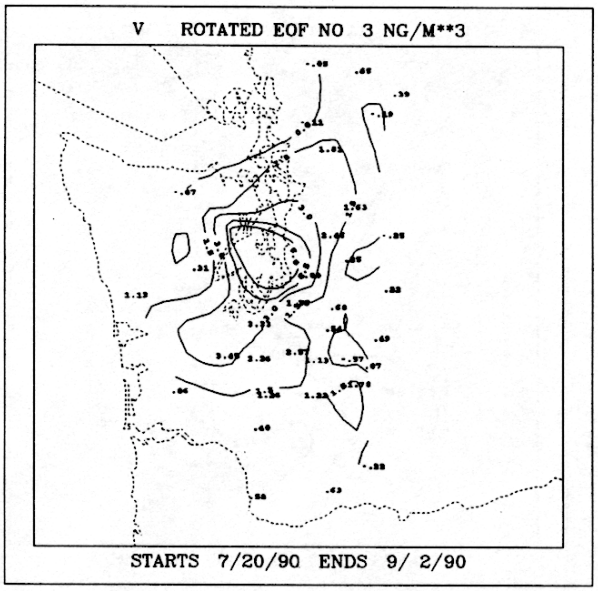

Figure 11-55. Rotated EOF 3 for vanadium explaining 6.0% of the variance. Contour interval is 1.5 ng/m^3.

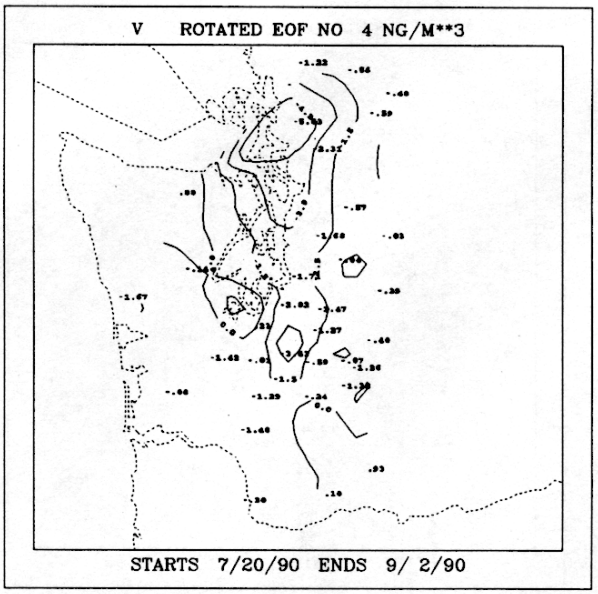

Figure 11-56. Rotated EOF 4 for vanadium explaining 5.9% of the variance. Contour interval is 1.5 ng/m^3.

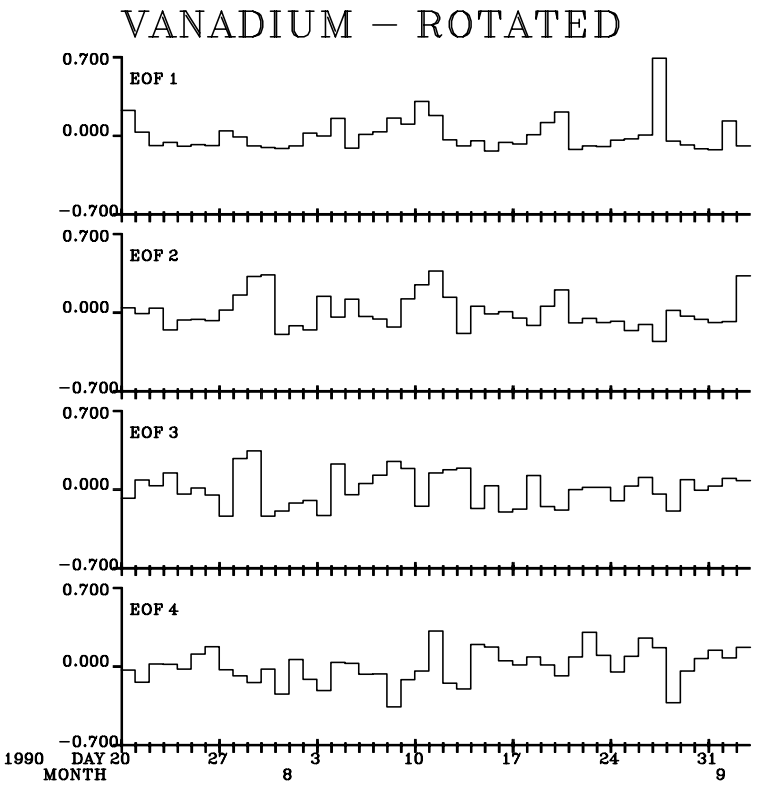

Figure 11-57. Time factors for the first four rotated EOFs for vanadium.

11.5.11 Lead

The highest lead concentration measured during the analysis period was 118 ng/m^3 at Puyallup on August 25. This is more than a factor of 3 higher than the next highest concentration, 39 ng/m^3. There is no reason to believe that it is invalid data. However, it was not included in the EOF analysis in order to better see the overall patterns in the lead concentrations. If the data point is left in, it dominates EOF 1, i.e. this EOF has a time factor of nearly 1 on August 25 and nearly 0 on every other day and the spatial pattern shows a strong gradient around Puyallup.

A map of the mean lead concentrations (with August 25 at Puyallup removed) is shown in Figure 11-58. The highest mean concentration is 11.6 ng/m^3 at Puyallup, with values generally decreasing outward from there. Sauvie Island, near Portland, OR, is the exception. The mean concentration there is higher than at sites closer to the Seattle-Tacoma urban area.

Time plots of the lead concentrations at the receptor sites are shown in Figure 11-59. The highest concentration at any of the three sites was 28 ng/m^3 at Marblemount on August 26. There were no other concentrations at these three sites which were greater than 8 ng/m^3 during the EOF analysis period. The highest lead concentration at Tahoma Woods was 7.7 ng/m^3 on August 20. The highest at Paradise was only 4.2 ng/m^3 on August 28.

Nine EOFs explaining 93.7% of the variance were rotated for lead. The first four are shown in Figures 11-60 through 11-63, with the time factors in Figure 11-64. EOFs 1 and 2 have the strongest gradients around Puyallup, with the gradient on EOF 2 being greater than for EOF 1. EOF 3 has a strong gradient around Cowlitz, which is south of Centralia, but the time factors show that this pattern existed on only one day, August 27, when the concentration at

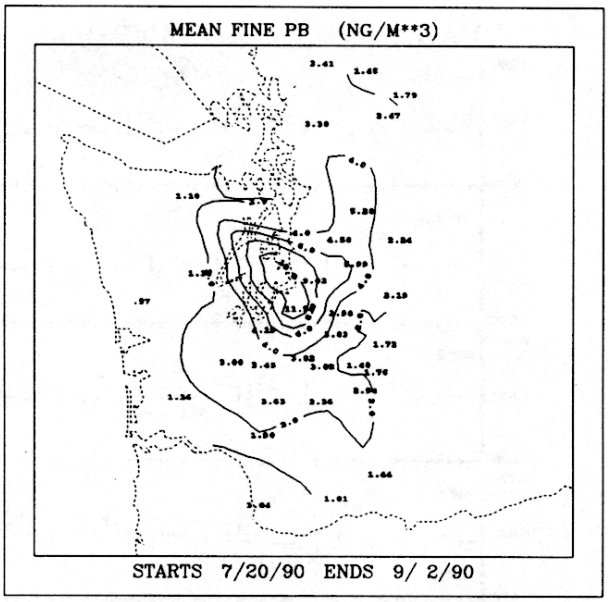

Figure 11-58. Mean lead concentrations excluding August 25 at Puyallup. Contour interval is 2 ng/m^3.

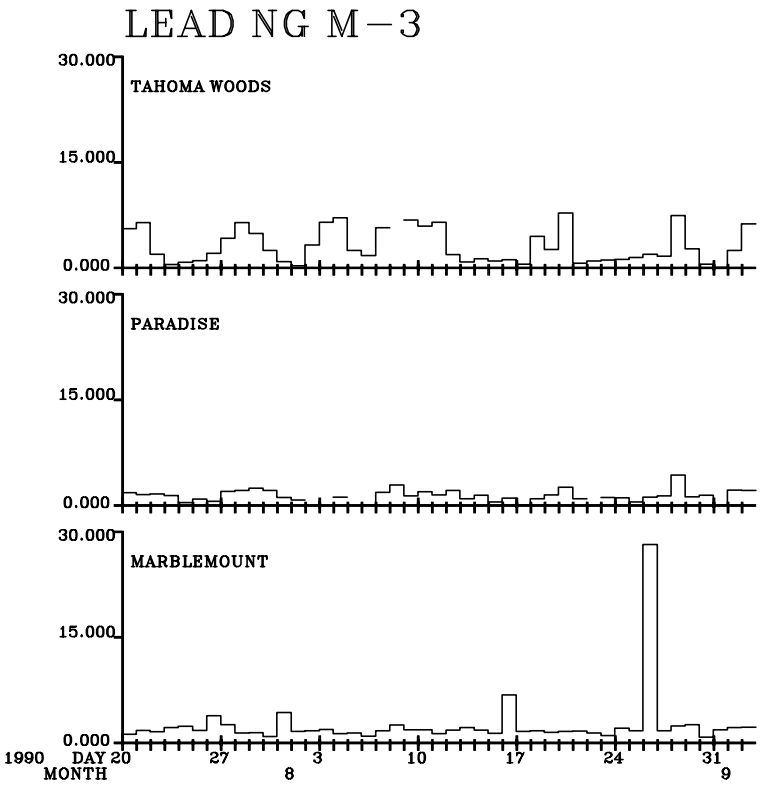

Figure 11-59. Lead concentrations at the receptor sites.

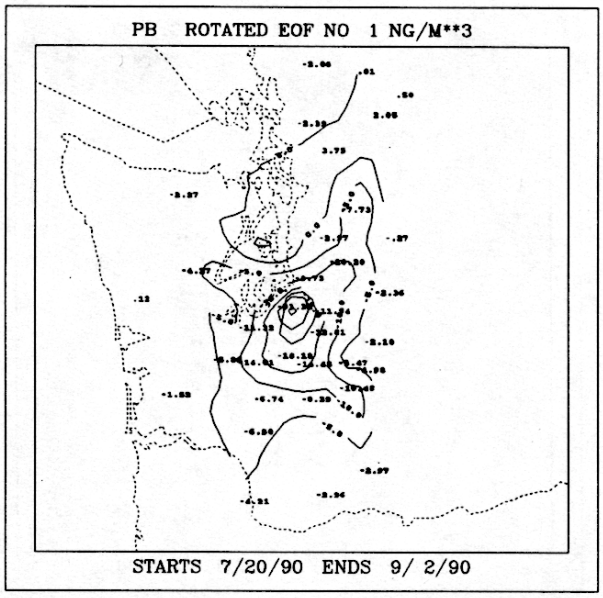

Figure 11-60. Rotated EOF 1 for lead explaining 22.7% of the variance. Contour interval is 5 ng/m^3.

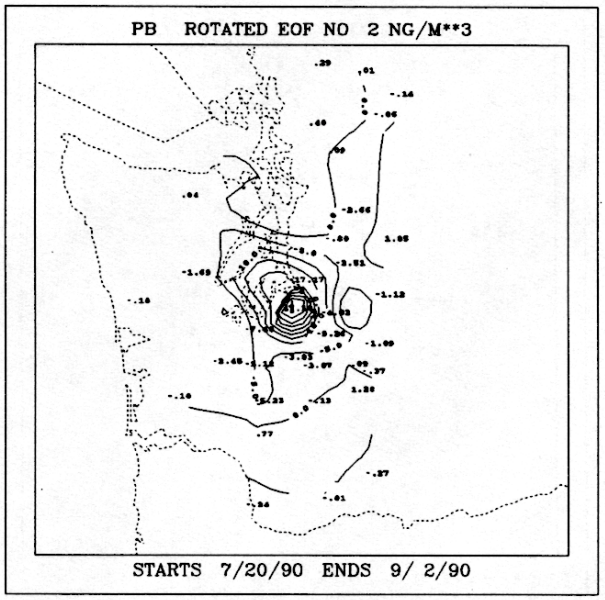

Figure 11-61. Rotated EOF 2 for lead explaining 22.1% of the variance. Contour interval is 5 ng/m^3.

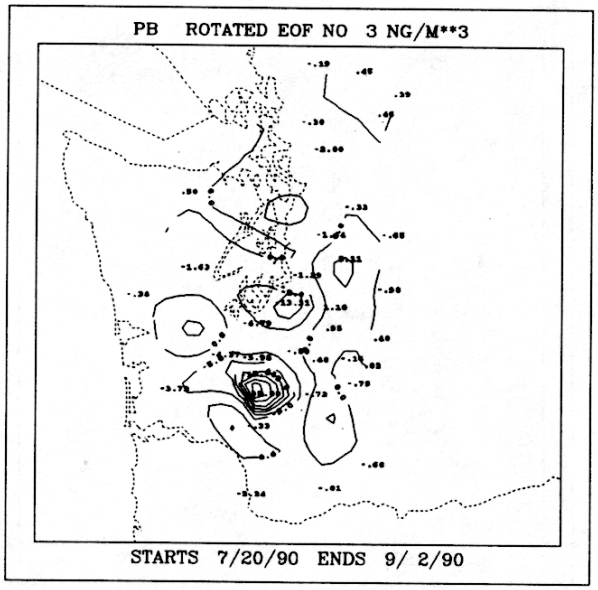

Figure 11-62. Rotated EOF 3 for lead explaining 12.7% of the variance. Contour interval is 5 ng/m^3.

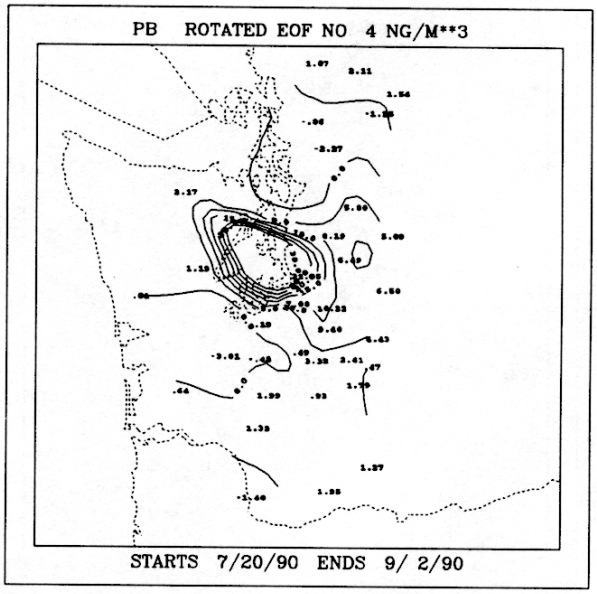

Figure 11-63. Rotated EOF 4 for lead explaining 11.0% of the variance. Contour interval is 5 ng/m^3.

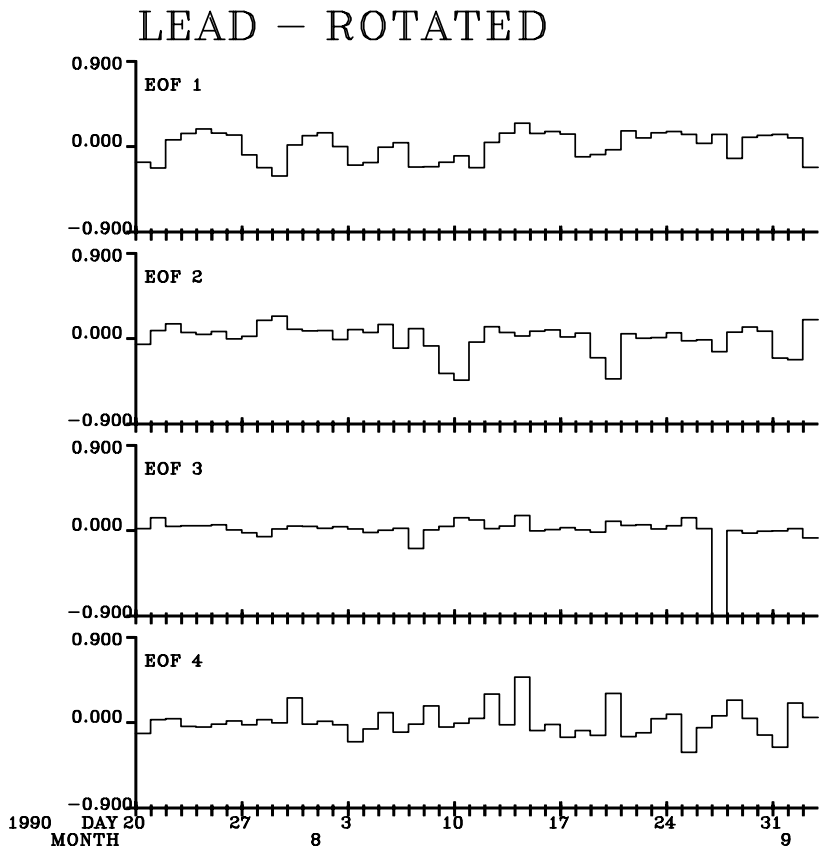

Figure 11-64. Time factors for the first four rotated EOFs for lead.

Cowlitz was 39 ng/m^3. All other lead concentrations at this site were less than 9 ng/m^3. The gradient in EOF 4 is centered around Kent, which is just north of Puyallup. EOF 5 (not shown) has a gradient around Marblemount in North Cascades National Park, but as for EOF 3, the time factors show that this pattern dominated on only one day, in this case, August 26 when the lead concentration at Marblemount was 28 ng/m^3.

11.5.12 Zinc

The three highest zinc concentrations measured were 164 ng/m^3 at Carson, on the southern edge of the network near the Oregon border, on July 30, 61 ng/m^3 at Kent on August 20, and 59 ng/m^3 at Carson on August 28. The 61 ng/m^3 at Kent is not unusually high compared to the concentrations measured there during the rest of the study. However, the two high concentrations at Carson are unusual for this site. All other concentrations during the analysis period at Carson were less than 8 ng/m^3, although two values higher than this were measured there on July 8 (21 ng/m^3) and July 4 (11 ng/m^3) which were during PREVENT, but not during the spatial and temporal trends analysis period. EOF analyses were done both including and not including the highest concentration, but only the values including it are presented here. As will be discussed below, the two high days at Carson load onto the EOFs in such a manner as to be easily distinguishable and therefore are presented. The map of mean zinc concentrations is presented in Figure 11-65. If the highest concentration at Carson is not included, the mean there drops from 8 to 4 ng/m^3. The highest mean zinc concentrations are around the Seattle-Tacoma urban area, including 15 ng/m^3 at Kent and 12 ng/m^3 at Puyallup; and at Sauvie Island (9 ng/m^3) which is near the Oregon border.

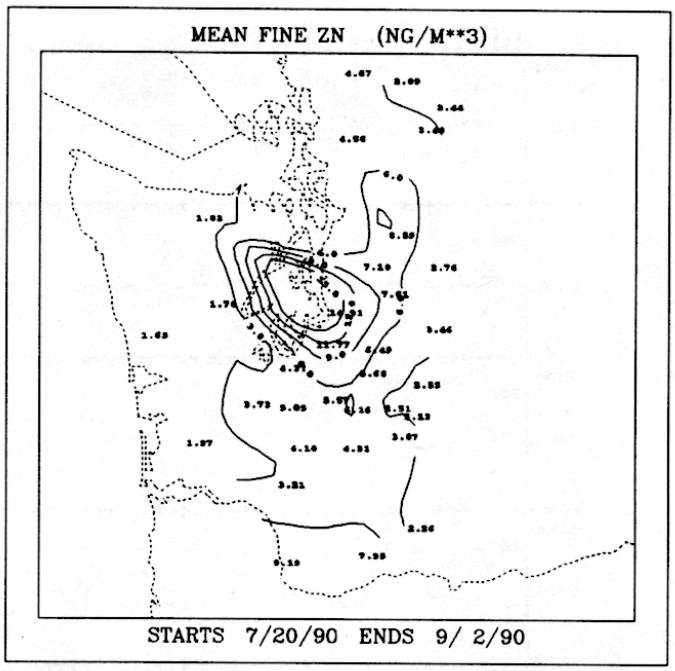

Figure 11-65. Mean zinc concentrations. Contour interval is 3 ng/m³.

Time plots of the zinc concentrations at the receptor sites are shown in Figure 11-66. The temporal patterns at Tahoma Woods and Paradise are similar, although the concentrations are higher at Tahoma Woods. The highest concentration there was 18 ng/m^3 on August 4. Data for Paradise was missing for this day. The highest zinc concentration at Paradise was 9 ng/m^3 on August 28. The concentration at Tahoma Woods on the same day was 16 ng/m^3 which was the second highest value measured there. The highest zinc concentration at Marblemount was 12 ng/m^3 on July 23.

Nine EOFs explaining 95.0% of the variance were rotated for zinc. The first four are shown in Figures 11-67 through 11-70, with the time factors in Figure 11-71. The first EOF loads most strongly on July 30 and is a consequence of the high concentration at Carson on this day. The gradient for EOF 1 is not only strongest around Carson, but also shows a gradient around the urban area. The second and third EOFs also show gradients around the urban area, as do EOFs 7 and 8 (not shown). The gradient around Carson on EOF 3 is mostly due to the second highest concentration measured there on August 28. EOFs 4 and 5 (5 not shown) show relatively weak gradients around several sites which are south of the urban area, but north of Sauvie Island. EOFs 4 and 5 also indicate that there may be transport of zinc from the south into the study area.

11.5.13 Copper

Copper concentrations were much more episodic than were the concentrations of any other element, i.e. copper concentrations at many sites were quite low except for one or two days when the concentration was several times higher than the remainder of the days at that site. For this reason, EOFs of copper are not presented. Many EOFs loaded onto a single site for a single day and thus were not very informative except to confirm that high concentrations were quite episodic. The episodicity may be physically real or may be due to the copper concentrations often being near the MDL.

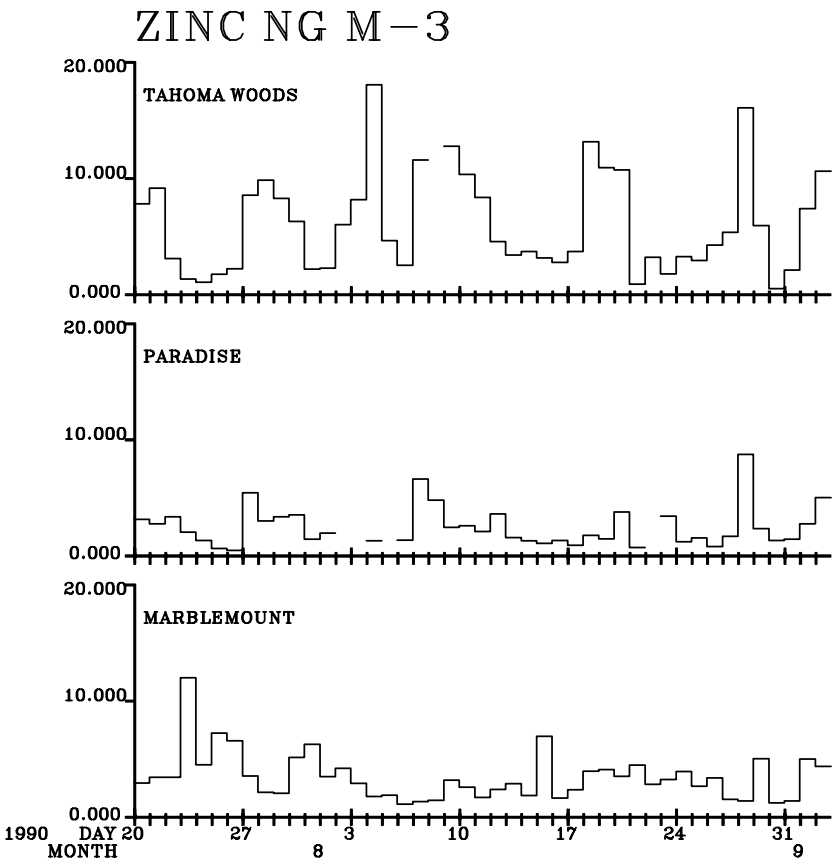

Figure 11-66. Time line of fine zinc at the three receptor sites.

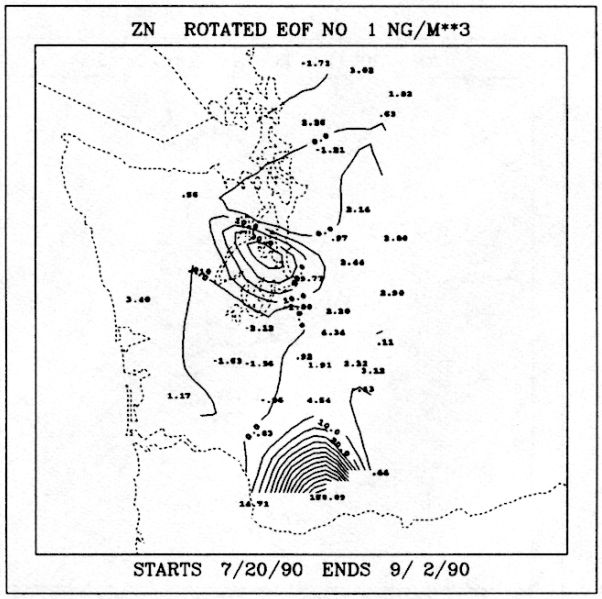

Figure 11-67. Rotated EOF 1 for zinc explaining 49.4% of the variance. Contour interval is 10 ng/m^3.

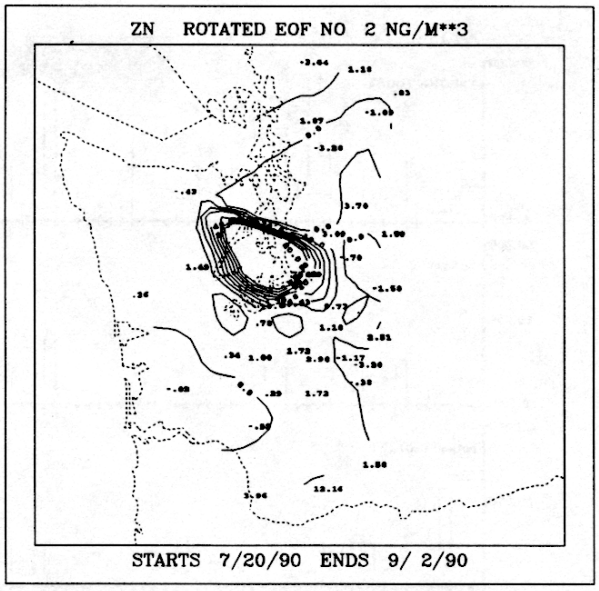

Figure 11-68. Rotated EOF 2 for zinc explaining 21.3% of the variance. Contour interval is 10 ng/m^3.

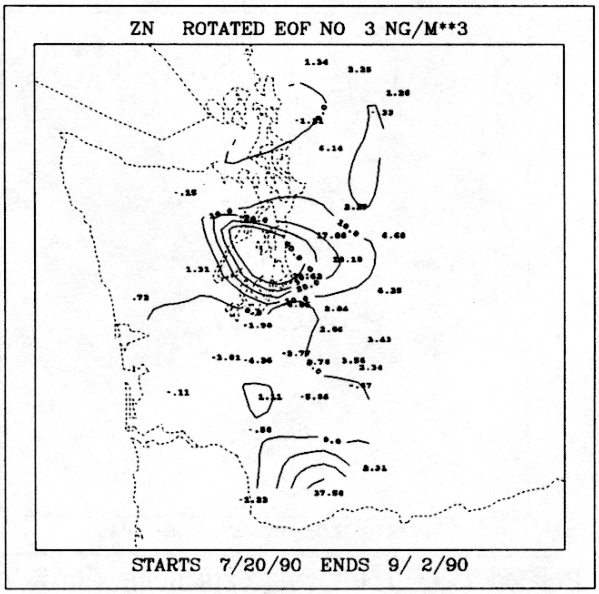

Figure 11-69. Rotated EOF 3 for zinc explaining 6.6% of the variance. Contour interval is 10 ng/m^3.

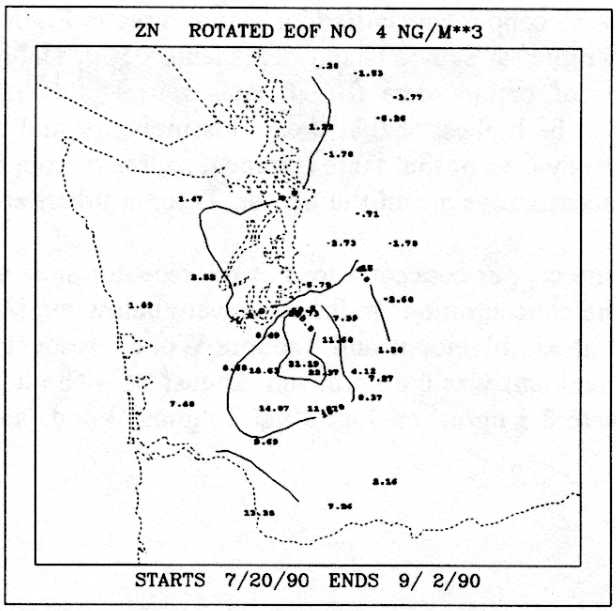

Figure 11-70. Rotated EOF 4 for zinc explaining 6.3% of the variance. Contour interval is 10 ng/m^3.

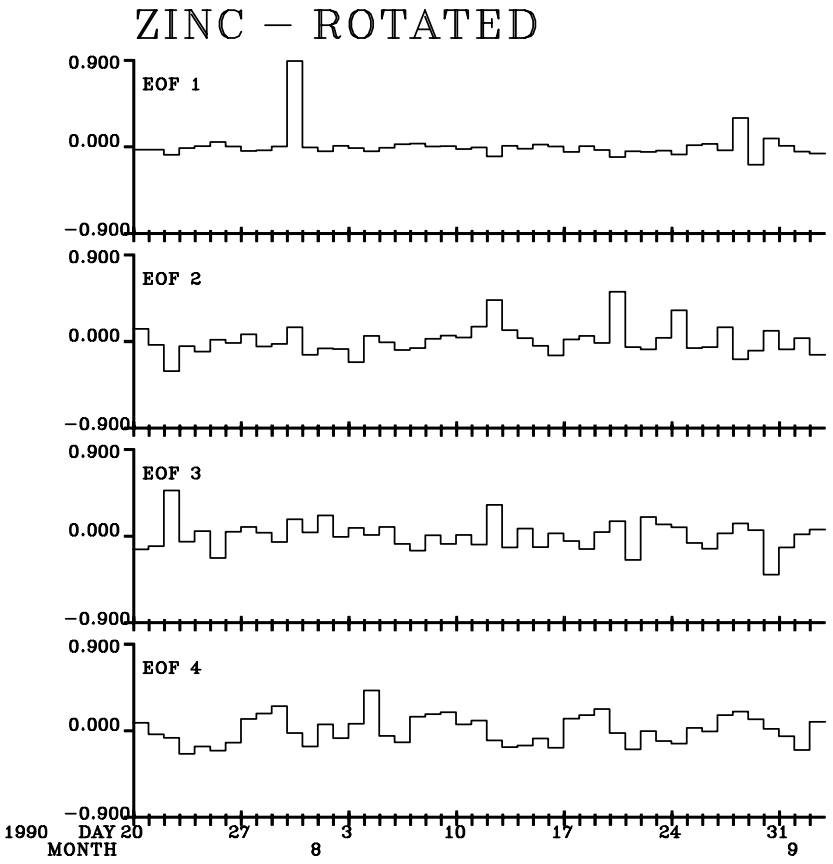

Figure 11-71. Time factors for the first four rotated EOFs for zinc.

A map of the mean copper concentrations is presented in Figure 11-72. The highest mean concentration was 2.75 ng/m^3 at Sauvie Island. This feature is probably real because a qualitative look at the time lines of copper data for all sites reveals that on a day to day basis the concentrations appear to be highest at this site. This indicates that copper may be transported from Oregon into the study area or that there is a local source of copper in or near Portland. The next highest mean concentrations are in the Seattle-Tacoma urban area.

Time plots of the copper concentrations at the receptor sites are shown in Figure 11-73. More than a third of the concentrations at Paradise were below the MDL, but only 7% and 13% were below the MDL at Marblemount and Tahoma Woods, respectively. The highest copper concentration at Marblemount was 6.6 ng/m^3 on August 15. The highest concentrations at the Mount Rainier sites were 3.5 ng/m^3 on July 30 at Tahoma Woods and 2.8 ng/m^3 on August 23 at Paradise.

11.6 DISCUSSION

Several hypotheses can be formed about the sources and transport patterns of the fine mass measured in western Washington State during the summer of 1990 based on analyses of the spatial and temporal patterns of the major constituents of the mass, including sulfates, organic matter, and b_{abs}. Some of these include:

1. The dominant spatial patterns associated with elemental sulfur concentrations indicate that Centralia Power Plant is probably not the only important source of sulfur in the region. The spatial pattern in the sulfur concentrations strongly suggests that other sources of sulfur in the Seattle-Tacoma urban area influence the sulfur concentrations in western Washington also. Sulfur concentrations in the northern half of the network appear to be influenced by sources farther north of Seattle. Transport from Canada or from Anacortes, WA, where there is oil refining, are possibilities.

2. The urban areas also appear to be associated with sources of organic matter. Although it appears that fires do produce significant quantities of organic carbon at individual monitoring sites over short time periods, there also appear to be some other sources of organics in or near the populated areas.

3. b_{abs} appears to be associated less with urban areas than either sulfur or organics and is likely to be more indicative of fires than is organic matter.

4. The highest concentrations of b_{abs}, organic carbon, and fine mass occasionally occur simultaneously at one or two sites over time periods as short as one day. These episodes appear to be associated with fires.

5. High concentrations of OMH do occur when the b_{abs} concentration is only about average. These time periods may be associated with fires, or there may be some other source type which causes high OMH concentrations.

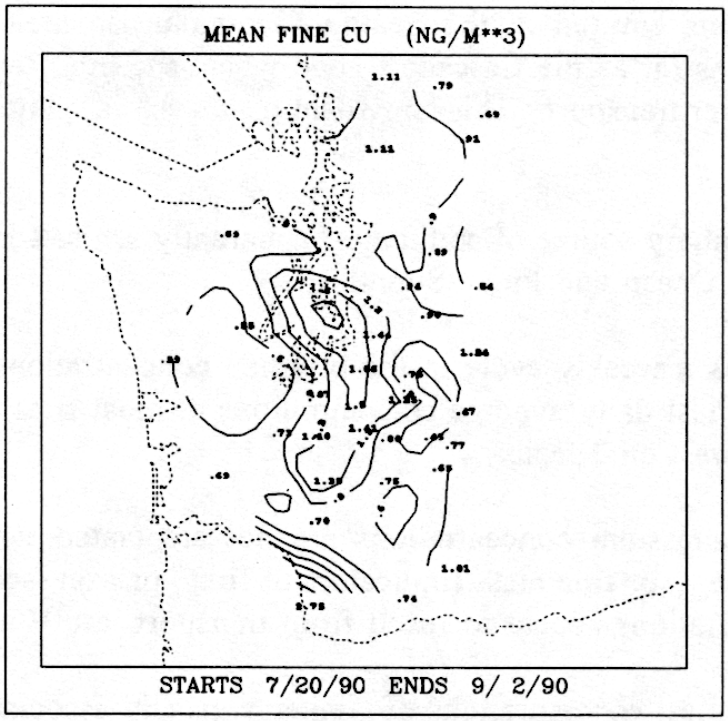

Figure 11-72. Mean copper concentrations. Contour interval is 0.3 ng/m³.

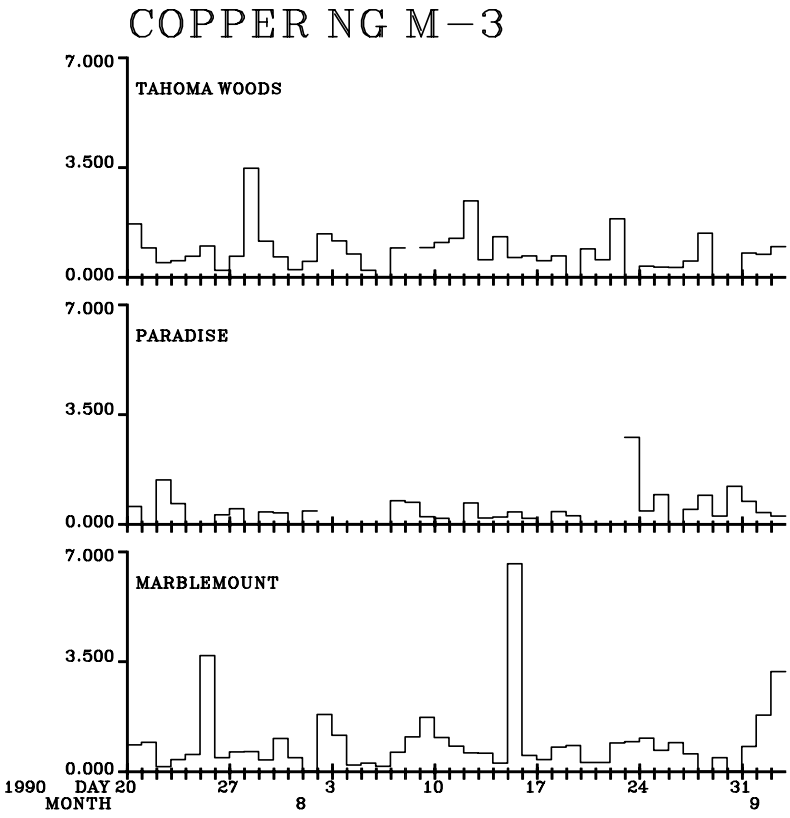

Figure 11-73. Copper concentrations at the receptor sites.

6. Pollutants emitted in the Seattle-Tacoma urban area appear to be transported inland as far as the Cascade Range where the high terrain then acts as a barrier to further transport. This is evident in the spatial patterns of sulfur, organics and b_{abs}.

7. The primary source of sodium is apparently sea salt transported inland from the Pacific Ocean and Puget Sound.

8. There is a weekly cycle in the bromine concentrations across the network, with the highest daily average concentrations at most sites being during the weekend and lowest on Tuesday.

9. High potassium concentrations are not associated with high concentrations of OMH, b_{abs}, or fine mass (indicators of fires) or iron (soil). The highest potassium concentrations appear to result from transport into Washington from Oregon.

10. The highest concentrations of elements usually associated with soil: iron, silicon, titanium, calcium, and aluminum were measured near Centralia Power Plant. It is possible that these species are associated with emissions from the plant rather than soil.

11. Several chemical species had absolute or relative maximums at Sauvie Island which is on the Oregon border near Portland. These include b_{abs}, potassium, vanadium, lead, zinc, and copper. This could be due to either some local industry near this monitoring site which emits these species, or could indicate transport of these species from somewhere in Oregon.

11.7 OPTICAL SCATTERING AND WIND TRAJECTORIES IN A REGIONAL MESOSCALE: THE PARTITION OF LOCAL AND REGIONAL EFFECTS BY EIGENVECTOR ANALYSES

An analysis of nephelometric optical scattering at seven sites in Washington State is reported here. Also, an interpolative model that displays winds and both forward and backward trajectories, derived from weather service data of the U.S. and Canada during the PREVENT period of June 6 through September 12, 1990 is described.

The data network is described in the following section. The nephelometry section expands upon the nephelometric data, correction for relative humidities, and inferences from an eigenvector decomposition of inter-site correlations among the measured optical scattering coefficients. The winds section describes a computer program that displays wind directions and trajectories during the PREVENT epoch, and summarizes certain statistics of the winds.

11.7.1 Data

For the PREVENT program Air Resource Specialists, Inc. (ARS), in cooperation with the National Park Service and the Washington State Department of Ecology, were responsible for

installation of meteorological and nephelometric monitoring instruments, and data logging and reporting at seven stations which are shown in Figure 2.2. The locations and altitudes of these sites are shown in Table 11-4.

At most sites, data were reported hourly between June 1, 1990 and September 4, 1990 for air and nephelometric chamber temperatures, barometric pressure, relative humidity, wind speed and direction, and the nephelometer scattering coefficient, b_{sp}. Further details of these data were reported in Chapters 2 and 3.

Table 11-4. Site names, code names, locations, and elevations of PREVENT nephelometer sites.

Site Name	Code	Latitude	Longitude	Feet ASL
Carbon River	CARN	47.0033	121.9881	1,650
Dog Mountain	DOGN	46.4997	122.1436	2,500
Marblemount	MARN	48.5333	121.4453	820
Newhalem	NEHA	48.6681	121.2983	1,600
Paradise	PARN	46.7119	121.7406	5,300
South Mountain	SOMO	47.3117	123.3933	3,000
Tahoma Woods	TAHN	46.7511	122.1211	1,428

11.7.2 Nephelometry

In this section we briefly report:

- Correction of the relative humidities measured outside the nephelometric scattering chambers to those expected within.
- Use of these corrected relative humidities to infer an approximate function to describe the effects of relative humidities on the optical scattering coefficients, b_{sp}.
- An eigenvector decomposition of the inter-site correlation matrix of the humidity-corrected b_{sp} at the seven sites.

11.7.2.1 Temperature Corrections For Relative Humidities

At most sites and times, the data record includes the ambient relative humidities (RH), and the ambient temperatures (T_a), and the temperatures within the scattering chamber (T_c). Assuming

that the mixing ratio of water vapor is unchanged by passage into the scattering chamber, the corrected relative humidities within the chamber (RH_c) are given by:

$$RH_c = RH \exp[T_w(T_a - T_c)/(T_a T_c)] \quad \textbf{(11-3)}$$

where T_w = [the latent heat of vaporization for water]/[the gas constant]
= 5210.5 K^o [averaged between 0 and 100 C^o]

When this transformation was applied to the raw RH data, relatively small corrections were appropriate at Tahoma Woods, Carbon River, and Marblemount, (where the nephelometers' input air was pre-heated), but larger corrections (10's of %) were required at the other sites.

An anomaly was noted among the corrected relative humidities, which occasionally exceeded 120%. This occurred when T_a was reported as *higher* than T_c and the ambient relative humidities were near 100. We arbitrarily top clipped all corrected relative humidities to 100%.

Figures 11-74 and 11-75 display scattergrams of the measured b_{sp} plotted against the corrected relative humidities, at one site each, for the pre-heated and unheated nephelometers.

11.7.2.2 Effects of Relative Humidity on b_{sp}

Figure 11-75 shows enhanced optical scattering at high relative humidities, a well-known effect that is observed when hygroscopic aerosols absorb water. Laboratory and field measurements with H_2SO_4 and $(NH_4)HSO_4$ aerosols have shown the curves of b_{sp} vs RH to approximate monotonic exponentials, as follows from Raoult's Law--mixing of continuously soluble acids and salts. With $(NH_4)_2SO_4$ a sharp and discontinuous step is observed at the deliquescence point for ammonium sulfate, near 70% RH. In favorable cases, these distinctive patterns have been resolved also with field measurements of poly-disperse aerosols.[6]

In field experiments the presence of ambient H_2SO_4 and NH_4HSO_4 aerosols have been confirmed by titrating the observed monotonic scattering functions to the characteristic deliquescent pattern of $(NH_4)_2SO_4$ by intentionally adding NH_3 to the nephelometric scattering chamber.[6]

The present scattergrams show no hint of a sharp deliquescence transition, which is not too surprising when all the points for all of the days are superimposed. At step-function break near 70% RH was also looked at. Marine air is generally impoverished of NH_3 (or, conversely, continental air is often "polluted" with it). It is likely that simple Raoult's Law behavior is operating here. If so, then with the (fairly good) assumption that b_{sp} is proportional to aerosol particles' volumes, one expects:

$$b_{sp}(RH) \approx \beta * M_s/(1 - RH/100) \quad \textbf{(11-4)}$$

where β is a constant that is inversely proportional to the product of the salt's van d'Hoff number and its molecular weight. M_s is the number-weighted average mass of solute particles in a poly-disperse aerosol.

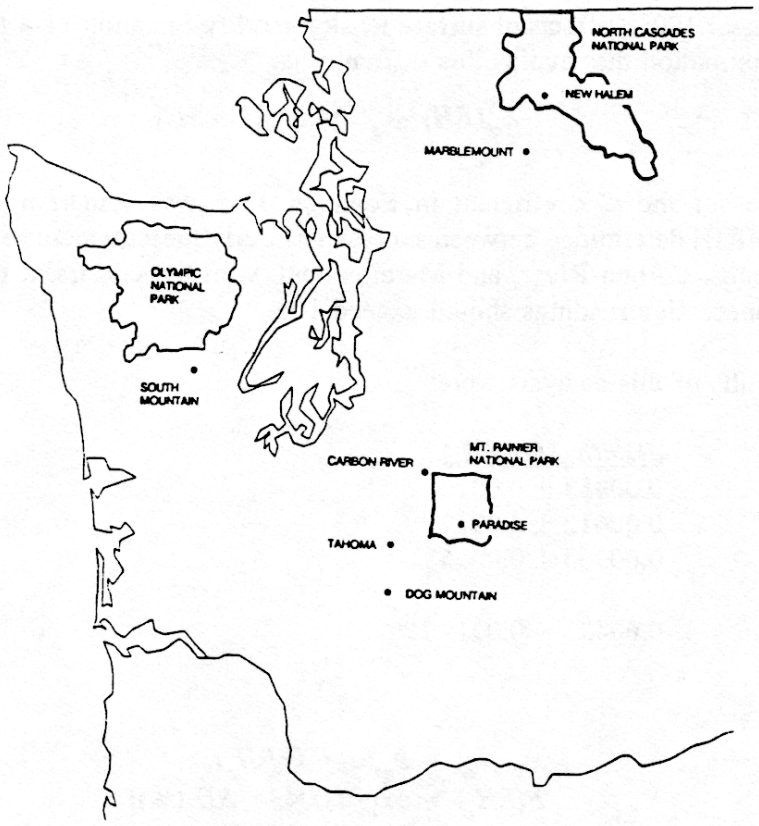

Figure 11-74. Site-location map for the b_{sp} and meteorological data stations reported in this study.

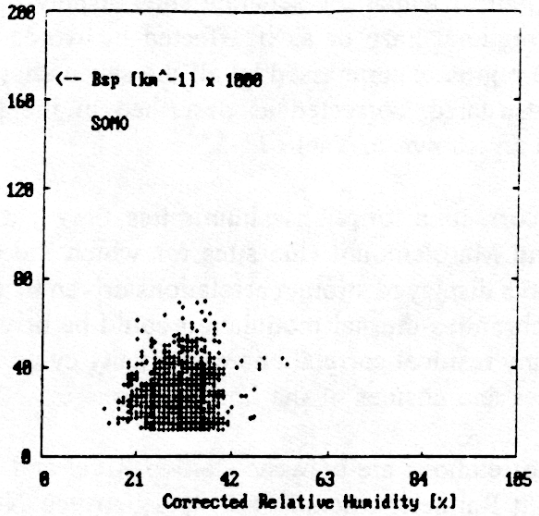

Figure 11-75. Scattergram of b_{sp} vs corrected relative humidities, RH_c at Marblemount.

At RH near 100%, effects of surface tension modify Equation 11-4 to prevent the infinity. A useful approximation that avoids this difficulty is:

$$b_{sp}(RH) \approx b_{sp}(0)^* \exp[C * RH] \qquad \textbf{(11-5)}$$

A value for the C coefficient in Equation 11-5 was sought by averaging values of $C \equiv d[Ln(b_{sp})]/d[\mathrm{RH}]$ determined between successive hourly measurements of b_{sp} and RH_c, for data at Tahoma Woods, Carbon River, and Marblemount, with the constraint that the differences in RH_c between successive readings should exceed 10%.

The results of this analysis were:

Station	$d[Ln(b_{sp})]/d[\mathrm{RH}_c]$
TAHN	0.00353 ± 0.0016
CARN	0.00612 ± 0.0017
MARN	0.00365 ± 0.0015
MEAN	0.00433 ± 0.0018

From which:

$$b_{sp} = b_{sp}(0)^* F(RH_c)$$
$$F(RH_c) = \exp[0.0043^* RH_c(\%)] \qquad \textbf{(11-6)}$$

The upper 1-σ, mean, and lower 1-σ limits on the $F(\mathrm{RH}_c)$ function at 100% corrected relative humidity, RH_c, are 1.85, 1.54, and 1.29, respectively.

11.7.2.3 Correlations and Eigenvectors

To explore the extent to which the separate sites display b_{sp} that vary coherently, as if immersed in a common regional haze or as if affected by winds or ventilations that may be common to the mesoscale region encompassed by all the seven sites, a cross correlation table of the b_{sp} readings was constructed, corrected as described in the previous section to relative humidities of 0%. These are shown in Table 11-5.

Note that without correction for relative humidities, the b_{sp} at several of the sites, Tahoma Woods, Carbon River, and Marblemount (the sites for which the chamber relative humidities varied strongly), would have displayed strong correlations driven by the diurnal relative-humidity cycle, and that other synchronous diurnal modulation could be driven also by the winds or ventilations. To remove any residual correlations with a daily cycle, two additional data columns were included for the sines and cosines of the hour angles.

The two highest correlations are between Carbon River and Tahoma Woods, both valley sites to the west of Mount Rainier National Park, and between Newhalem and Marblemount, neighboring sites in and near to the North Cascades National Park. Residual correlations with the sines and cosines of the daily hour angles are of mixed signs (quasi-random phases) and small

amplitudes.

Table 11-5. Intersite crossed correlation coefficients for b_{sp}.

	SOMO	DOGN	TAHN	PARN	CARN	MARN	NEHA	COS	SIN
SOMO	1.000	0.517	0.424	0.383	0.363	0.076	0.119	-0.081	-0.028
DOGN	0.517	1.000	0.569	0.483	0.492	0.137	0.177	0.017	-0.134
TAHN	0.424	0.569	1.000	0.350	0.769	0.249	0.186	0.152	0.040
PARN	0.383	0.483	0.350	1.000	0.366	0.082	0.173	0.038	-0.175
CARN	0.363	0.492	0.769	0.366	1.000	0.271	0.119	0.152	-0.072
MARN	0.076	0.137	0.249	0.082	0.271	1.000	0.705	0.127	0.027
NEHA	0.119	0.177	0.186	0.173	0.119	0.705	1.000	0.059	0.038
COS	-0.081	0.017	0.152	0.038	0.152	0.127	0.059	1.000	0.000
SIN	-0.028	-0.134	0.040	-0.175	-0.072	0.027	0.038	0.000	1.000

It is useful to seek linear combinations of the b_{sp} measurements that act as single, independent measurements that are uncorrelated with one another. To each of these combinations, or "eigenvectors," can be assigned an "eigenvalue" that is proportional to the fraction of the data variance that may be attributed to the corresponding vector.

Only the first four vectors (the left four numerical columns) subsume more of the data variance than would arrays of random numbers, and only the first two do so with significant confidence. Together, the two significant vectors account for half of all the variance, which is to say that the seven sites display half (or perhaps more) of their b_{sp} variations collectively, and half (or less) individually. The results of this analysis are presented in Table 11-6.

The first of the vectors shows approximately equal weights (0.362, 0.440, 0.467 ...) at each of the seven sites (South Mountain, Dog Mountain, Tahoma Woods, ...), as would be expected for a vector that approximates a simple average of the b_{sp} at every site. This vector may be imagined as a horizontal plane of b_{sp} that "heaves" uniformly throughout the modeled region. Alone, it accounts for about 35% of all the variance at all the sites.

The second vector loads the three southern mountain sites (South Mountain, Dog Mountain, and Paradise) about equally (0.235, 0.205, 0.192) and with opposite sense to the two strongly weighted (-0.639, -0.614) northern sites (Marblemount, Newhalem). This vector is insensitive to the southern valley sites (Tahoma Woods, Carbon River). It may be imagined as a b_{sp} plane that "tilts" on an axis running roughly NW to SE from Seattle to Walla Walla. Alone, it accounts for about 17% of all the variance at all the sites.

The third and fourth (marginally significant) vectors are respectively dominated by the sine and cosine, and by correlations between the two northern stations at Marblemount and Newhalem. Together, they account for 19% of all the variance.

Table 11-6. Results of eigenvector analysis of b_{sp} measurements from seven PREVENT sites.

Eigenvectors									
SOMO	0.362	0.235	0.207	0.235	0.265	0.672	0.265	0.235	0.015
DOGN	0.440	0.205	0.107	0.205	0.094	0.115	0.094	0.205	0.105
TAHN	0.467	0.063	-0.303	0.063	-0.304	-0.077	-0.304	0.063	-0.622
PARN	0.356	0.192	0.226	0.192	0.536	-0.622	0.536	0.192	-0.106
CARN	0.449	0.080	-0.294	0.080	-0.436	-0.186	-0.436	0.080	0.629
MARN	0.251	-0.638	0.130	-0.638	-0.156	0.046	-0.156	-0.638	-0.304
NEHA	0.237	-0.614	0.304	-0.614	0.136	0.010	0.136	-0.614	0.309
COS	0.083	-0.183	-0.682	-0.183	0.442	0.255	0.442	-0.183	0.028
SIN	-0.061	-0.196	-0.377	-0.196	0.335	-0.201	0.335	-0.196	0.077
Eigenvalues									
	3.119	1.568	1.092	1.032	0.720	0.569	0.433	0.273	0.194
Fractional Variances									
	0.347	0.174	0.121	0.115	0.080	0.063	0.048	0.030	0.022

The first four vectors collectively describe b_{sp} variations that are common to a mesoscale region that encompasses all the sites. They plausibly correlate with synoptically scaled features of the weather, such as "highs" and "lows," rather than with details of specific trajectories that connect sources and receptors.

The PREVENT program was mostly concerned with effects attributable to transport from place to place within the mesoscale, rather than with modulations common to the whole region. Thus only 25% or so of the b_{sp} variance appeared to carry information that was "useful" to this focus, with an upper limit of 50% if all four vectors were significant.

11.7.3 Winds

In this section we discuss:

- The wind data.
- "WHITHER," a computer model that displays interpolated wind fields and both backward and forward trajectories through receptor sites and suspected emission loci.

- Some statistics of the winds and inferences from an eigenvector decomposition of the wind variances.

11.7.3.1 The Wind Data

Air Resource Specialists, Inc. (ARS) collected meteorological data at Washington, Oregon, and British Columbia, including surface hourly weather observations for 52 sites, from the National Weather Services of the U.S. and Canada, surface hourly weather observations at 30 sites, from the USFS RAWS (AFFIRMS) network, and upper-level winds at eight sites, from the National Weather Service. Only the latter data were of sufficient resolution and quality to be useful for mesoscale wind interpolations. These were collated by ARS for NWS and Canadian rawind soundings reported twice a day (5AM and 5PM PDT) at eight stations listed in Table 11-7. A ninth station (Vancouver, YVR), which would have been useful as closely bounding the northern area the PREVENT study area, was unfortunately not available.

Table 11-7. Names, locations, codes of National Weather Service and Canadian rawinsonde stations.

Latitude	Longitude	Station	Code
47.57	124.33	Quillayute	UIL
47.38	117.32	Spokane	GEG
42.38	122.88	Medford	MFR
44.92	123.00	Salem	SLE
53.98	122.60	Fort Nelson	YVE
50.41	127.30	Port Hardy	YZT
53.88	121.68	Prince George	YXS
50.17	119.19	Vernon	WVK

In the section that follows we describe the use of these data for interpolative wind field displays.

11.7.3.2 Whither

To assist the attribution of visibility degradation at national parks, forests, and wilderness areas of the Pacific Northwest we have constructed a general purpose display module, WHITHER, that is implemented for DOS family microcomputers.

WHITHER interpolates rawinsonde wind data from eight stations in the Pacific Northwest and British Columbia. Surface winds are modified by a (somewhat dubious) low-order correction to account for effects of local topographic relief. Important temperature-gradient effects are unknown, and thus ignored.

WHITHER displays winds over the surface and at 3,000, 6,000, and 9,000 feet above sea level over the Pacific Northwest, during the period June 6, 1990 through September 13, 1990. These displays may be as evolving six-hr "movies," or as forward and backward trajectories through selected sites and times (Figures 11-76 and 11-77).

In Figure 11-76 the matrix of dots with their attached lines denote "arrows" (not flags), with the winds blowing along the shafts and toward the dots, with amplitudes proportional to the shaft lengths. An rms velocity scale is given in the lower right corner. To reduce screen clutter, winds are displayed at only every third grid element of a 60x45 matrix.

In Figure 11-77, both forward and backward trajectories were plotted through the central dense circle, starting at the date and time listed at the foot of this figure. Smaller circles are located along the trajectory at 30-minute intervals. Larger open circles are located at 12-hour intervals. Winds are interpolated in both time and space.

11.7.3.3 Wind Statistics

In this section we discuss:

1. The cumulative vector winds at the eight sounding sites and their erratic "Ekman" rotations.

2. Inferences from an eigenvector decomposition of the correlations in the near surface wind amplitudes at the eight sites.

Figures 11-78 and 11-79 illustrate a polar scattergram at the surface and a cumulative trajectory at 3,000 feet above Quillayute, during the interval June 6, 1990 through September 6, 1990. Think of the scattergram as an enhanced wind-rose diagram, with each dot pointing *upwind*, with a radius proportional to a sounding's velocity, at the surface. Think of the cumulative trajectory as a track (seen from above) of a fictitious neutral-buoyancy balloon floating in the winds recorded at a site, at a specified height. Obviously, wind rotations in both senses occur and are affected by near-surface topography and temperature gradients. The net vector winds summarized in Table 11-8 are, in effect, direction averages that are weighted by the wind speeds. The rotation angles and velocity changes for these winds are summarized in Table 11-9. Note the large standard deviations for the rotation angles. It is clear that both topography and near-surface horizontal temperature gradients dominate the lower-level winds at these sites.

11.7.4 Eigenvectors

The preceding paragraphs summarize the difference between the surface winds and those at upper levels, at individual sites. The emphasis of this discussion so far has been that local effects of temperature and topography strongly affect these differences but to unknown relative effect.

It is useful now to explore the extent to which both the upper and lower level winds behave in ways that are experienced by all stations in common, and the extent to which they are affected by local physics, only.

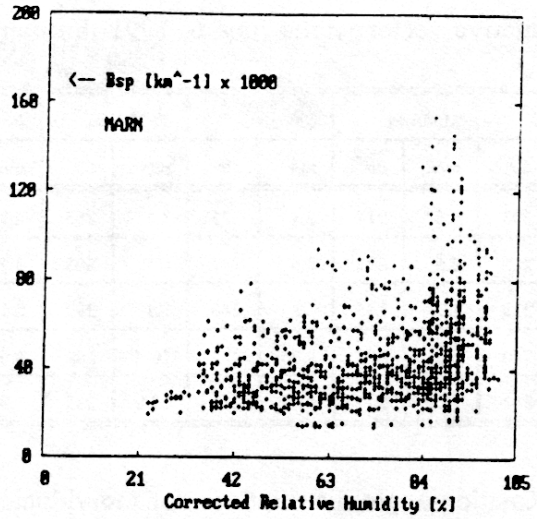

Figure 11-76. Surface-level winds estimated by WHITHER on June 7:00:00 PDT. Winds blow towards the arrow heads with velocities proportional to the lengths.

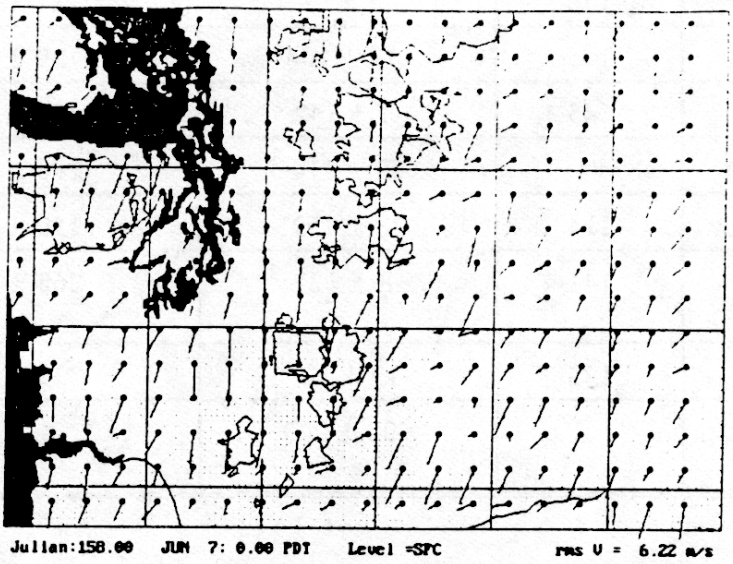

Figure 11-77. A surface wind trajectory estimated by WHITHER. The curve to the lower left is backwards for 24 hours; that to the top is forwards. The receptor is at 47.4972 N., 121.9953 W. on June 6:12:00 PDT.

Table 11-8. Cumulative vector winds June 6, 1991 through September 13, 1991.

kraft	Quillayute		Spokane		Medford		Salem		Ft Nelson		Port Hardy		Pr George		Vernon	
ASL	m/s	dir	m/s	dir	m/s	dir	m/s	dir	m/s	dir	m/s	dir	m/s	dir	m/s	dir
000	2.3	272	2.5	203	4.6	317	2.1	325	1.1	263	2.7	320	1.6	269	2.6	196
003	2.1	254	2.7	219	4.6	302	3.5	337	6.1	303	3.7	307	4.9	287	3.2	261
006	3.1	243	5.5	238	1.7	245	3.3	240	9.1	297	2.5	234	5.4	269	2.6	258
009	6.0	243	8.7	240	8.5	208	8.0	222	10.4	289	4.6	241	8.1	253	6.7	238
012	9.6	242	13.8	241	12.7	214	11.7	223	13.9	285	6.8	238	10.1	252	10.5	242

Table 11-9. Rotation-angle distributions for individual soundings at 0z.

Station	npts	Rotation 12,000'-SFC Degrees	Velocity Change 12,000-SFC Percent
Quillayute	152	-10 ± 105	205 ± 282
Spokane	156	45 ± 99	127 ± 180
Medford	165	-77 ± 106	129 ± 120
Salem	145	-1 ± 142	199 ± 237
Ft Nelson	81	82 ± 114	298 ± 405
Port Hardy	114	30 ± 152	150 ± 232
Prince George	141	-8 ± 121	268 ± 361
Vernon	122	-13 ± 128	339 ± 287
"Ekman Spiral"	...	+90 ± 000	... ...

One way to do this is to form matrices expressing the correlation between the U and V components of the winds at the different sites, and then to seek linear combinations (or "eigenvectors") of the observations that best subsume the variations of the network at large. Then collecting the most significant of those vectors, one can approximate the fraction of all the variation that can be "explained" in terms of collective behavior, and by difference estimate the fraction that must be explained by local behavior, only. The results of such an analysis are given in Table 11-10.

Table 11-10. Coherence fractions for the surface and upper-level winds at eight sites in the Pacific Northwest.

Altitude and Wind Direction	All Stations in Common (Synoptic Effects)	Stations Individually (Local Effects)
Surface (U)	61.3%	38.7%
(V)	63.9%	36.1%
3000 ft (U)	63.0%	36.1%
(V)	60.4%	39.6%
6000 ft (U)	66.7%	33.3%
(V)	55.8%	44.2%
9000 ft (U)	71.2%	28.8%
(V)	64.7%	35.3%
12000 ft (U)	61.7%	38.3%
(V)	70.1%	29.9%
Averages	63.9%	36.1%

Unlike the discussion of the former section, where no generalization could be made about the sense of wind-vector rotations as functions of altitude above the surface, the present analysis presents a robust conclusion that:

At all levels for these eight sites, about two-thirds of the temporal variations behave as if a coherent property of all the stations, and one-third as if dominated by local physics, only.

Thus while the local horizontal temperature gradients and relief may together account for about one-third of those large rotation deviations, it is still hoped that about two-thirds of them may be accounted for at any local site by interpolation of data collected at several more or less distant sites.

11.7.5 Summary and Discussion

By eigenanalyses of both b_{sp} and wind velocities it is estimated that half or more of the measurement variances at the eight sites of this study may be attributed to mesoscale physics that affect the network as a whole, with the remainder attributable to "local" effects.

For b_{sp} in this partition, "mesoscale" effects may include both "regional haze" and regionally synchronous stagnation events that by diminishing the ventilation may exacerbate the effects of locally emitted light-scattering aerosols. In this context, "local" effects may include both local emission and ventilation fluctuations that are not characteristic of the network as a whole, and the transport to local receptors of emissions from more distant sources by discretely targeted plumes.

Thus it appears that less than half of visibility impairment at these rural sites can be directly attributed to discrete plumes from upwind urban sources, during the interval of this study.

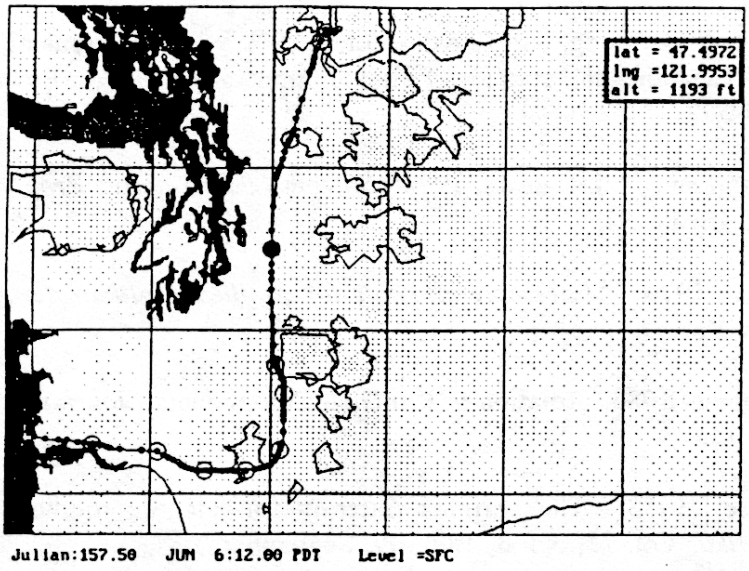

Figure 11-78. Polar scattergram of twice-daily (0z and 12z) surface winds at Quillayute, June 6 - September 13, 1990. The radius vector for each dot points upwind, with amplitude 4 m/s circle.

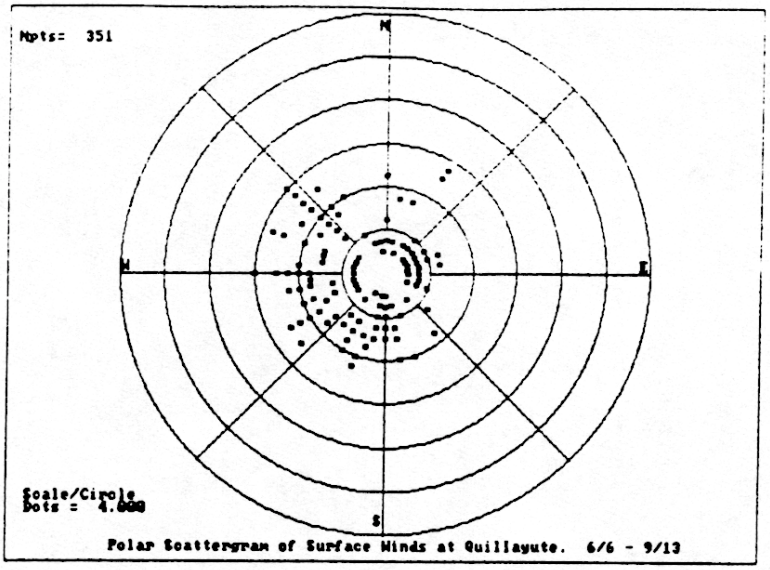

Figure 11-79. Cumulative trajectory for winds at 3000' above Quillayute, June 6 - September 13. The sawtooth pattern reflects alternating "high" and "low" synoptic weather systems.

REFERENCES

1. R.C. Henry, Y.-J. Wang, and K.A. Gebhart, 1991. The relationship between empirical orthogonal functions and sources of air pollution. *Atmospheric Environment*, Vol. 25A, No. 2, 503-509.

2. C. L. Lawson and R. J. Hanson, 1974. *Solving Least Squares Problems*, Princeton-Hall, Englewood Cliffs, NJ.

3. P. E. Green, 1976. *Mathematical Tools for Applied Multivariate Analysis*, Academic Press, New York.

4. M. B. Richman, 1986. Rotation of Principal Components. *Journal of Climatology*, Vol. 6, pp. 293-335.

5. H. F. Kaiser, 1958. The varimax criterion for analytic rotation in factor analysis. *Psychometrika*, Vol. 23, No. 3, 187-199, September.

6. R.J. Charlson, A.H. Vanderpol, D.S. Covert, A.P. Waggoner, and N.C. Ahlquist. "Sulfuric Acid and Ammonium Sulfate Aerosols..." *Science*, Vol. 184, pp. 156-158.